THESIS FOR THE DEGREE OF LICENTIATE OF ENGINEERING

Microstructural Characterization of Expanded Austenite in 304L and 904L Austenitic Stainless Steels

Giulio Maistro

Department of Materials and Manufacturing Technology
CHALMERS UNIVERSITY OF TECHNOLOGY
Gothenburg, Sweden 2015

Microstructural Characterization of Expanded Austenite in 304L and 904L Austenitic Stainless Steels
GIULIO MAISTRO

ISSN 1652-8891
Technical report no 102/2015

Department of Materials and Manufacturing Technology
Chalmers University of Technology
SE-412 96 Gothenburg
Sweden
Telephone + 46 (0)31-772 1000

Printed by Chalmers Reproservice
Gothenburg, Sweden 2015

Microstructural Characterization of Expanded Austenite in 304L and 904L Austenitic Stainless Steels

Giulio Maistro

Department of Materials and Manufacturing Technology
Chalmers University of Technology

Abstract

Austenitic stainless steels are among the most used materials in modern industry, mainly because of their superior corrosion resistance. However, low hardness and poor tribological properties often restrict their applicability. Conventional surface hardening techniques such as high-temperature carburizing (T > 850°C) and nitriding (T > 550°C) are not applicable to these alloys. Rapid precipitation of chromium-rich carbides/nitrides at the grain boundaries would in such cases induce chromium depletion in the alloy and compromise the corrosion resistance.

Since the middle of the ´80s, low-temperature thermochemical treatments (T < 500°C) were developed for surface hardening of austenitic stainless steels, including gas carburizing and plasma nitriding. These processes can induce formation of a precipitate-free interstitially supersaturated metastable expanded austenite, also known as S-phase, having superior hardness (800-1500 HV), and improved wear resistance while maintaining corrosion resistance.

In this study, industrial low-temperature carburizing and nitriding were performed on two austenitic stainless steels, 304L and 904L. The focus of this thesis is the material response to these low temperature treatments and thermal stability of the metastable structure formed. The aim is to investigate the influence of the alloy composition and surface finishing as well as thermal annealing on the microstructure, phase constituents, strain evolution and hardening effect of the modified layer by means of combined analytical techniques such as XPS, XRD, SEM, GDOES and EBSD.

It has been found that surfaces with a high amount of plastic deformation (original surface finishing) show higher supersaturation of interstitials, generally accompanied by a faster diffusion of interstitials and thicker expanded austenite case layer. The formation of expanded austenite is accompanied by carbides/nitride for as-carburized 304L. However, the highly alloyed 904L exhibits mainly S-phase with larger degree of lattice expansion. Presence of ferrite/martensite make the formation of S-phase less favorable and might promote nitride/carbide precipitation in 304L. It has also been found that the expanded austenite decomposes upon vacuum annealing (600°C for 150 h) following a eutectoid route for 304L and a discontinuous route for 904L. Low temperature treatment induced significant enhancement of surface hardness, more effectively on 904L. The hardening mechanisms have also been discussed.

Keywords: Expanded austenite, S-phase, low-temperature thermochemical treatment, austenitic stainless steel, surface engineering, surface analysis, XPS, XRD, SEM, EBSD, GDOES, thermal stability

Preface

This licentiate thesis is based on the work performed in the Department of Materials and Manufacturing Technology between January 2013 and September 2015. The project has been carried out under the supervision of Associate Professor Yu Cao and Professor Lars Nyborg.

The thesis consists of an introductory part followed by the appended papers:

Paper I: Multi-technique characterization of low-temperature plasma nitrided austenitic AISI 304L and 904L stainless steel
Y.Cao, G. Maistro, M. Norell, S. A. Pérez-Garcia and L.Nyborg
Surface and Interface Analysis, 46 (10-11) pp. 856-860

Paper II: Microstructural characterization and layer stability of low-temperature carburized AISI 304L and AISI 904L Austenitic Stainless Steel
G. Maistro, L. Nyborg, S. Vezzù, Y. Cao
Accepted for publication in La Metallurgia Italiana, 2015

Paper III: Application of EBSD for strain analysis and microstructural evaluation of low-temperature carburized austenitic stainless steels
G. Maistro, C. Oikonomou, L. Rogström, L. Nyborg, Y. Cao
Manuscript. Submitted for publication in Surface and Interface Analysis special issue, 2015

Contribution to the appended papers

Paper I. The author conducted part of the experimental work, participated in paper writing and corrections.

Paper II. The author planned and executed the experimental work as well as data analysis. GDOES measurements were performed by Dr. Simone Vezzú. The author wrote the paper.

Paper III. The author planned and executed the work in cooperation with the co-authors. EBSD measurements were performed by Lic. Eng. C. Oikonomou. Nano-indentation measurements were performed by Dr. L. Rogström. The author wrote the paper.

List of acronyms and abbreviations

Ann: annealed

ASS: austenitic stainless steel

BCC: body-centred cubic

EBSD: electron backscattered diffraction

EDX: energy dispersed x-ray spectroscopy

FCC: face-centred cubic

GDOES: glow-discharge optical emission spectroscopy

GIXRD: grazing incidence x-ray diffraction

LOM: light optical microscopy

LTC: low-temperature carburizing

LTN: low-temperature nitriding

LTTT: low-temperature thermochemical treatment

K22: low-temperature carburized with Kolsterising K22 process

NP: non-polished

P: polished

PN: plasma nitriding

SEM: scanning electron microscopy

SF: stacking fault

S-phase: expanded austenite

SS: stainless steel

XPS: X-ray photoelectron spectroscopy

XRD: X-ray diffraction

y_N, y_C: nitrogen/carbon interstitial occupancy

γ_N, γ_C; nitrogen/carbon stabilized expanded austenite

Table of contents

1 Introduction

1.1 Background

Austenitic stainless steels (ASS) are among the most used materials where high corrosion resistance is required, with applications ranging from pharmaceutical and food industry to offshore oil and gas, passing through biomedical and prosthetics. The presence of Cr as an alloying element guarantees a stable protective oxide. Anti-corrosion properties are also enhanced by presence of Ni as austenite stabiliser, which gives ASS a face-centred cubic (FCC) structure.

The major drawbacks of this class of materials are the low surface hardness and poor wear resistance, leading to high risk of galling. Although it is possible to effectively harden ASS surfaces by inducing plastic deformation thanks to the high work-hardenability, this tends to decrease the general corrosion resistance especially in chlorine containing environments, due to high susceptibility to stress corrosion cracking.

Traditional thermochemical treatments used to case-harden steels are not suitable for ASS due to the high temperatures involved in the processes. Carburizing and nitriding are commonly carried out at temperatures above 850°C and 500°C respectively. Due to high affinity to nitrogen/carbon, Cr depletion caused by rapid precipitation of Cr-rich carbides/nitrides leads to severe decay in corrosion resistance of the materials.

From the mid-80s, low-temperature thermochemical treatments (LTTT) involving both nitrogen and carbon were developed and attracted interest from both academia and industry. Such low-temperature processes induce the formation of a metastable interstitially super-saturated austenite phase, referred to as *expanded austenite* or *S-phase*. The interest in expanded austenite is due to the interstitial content, orders of magnitude higher than the thermodynamic equilibrium and the absence of precipitates. These two factors assure up to a four to five-fold increase in hardness while maintaining or even enhancing the pristine corrosion resistance.

Expanded austenite is an intrinsically complex structure. Being metastable, thermodynamic calculations cannot effectively predict temperature and compositional ranges of stable S-phase. Moreover, as a result of the diffusion process, it is characterized by high concentration gradients between an often present surface compound layer and the interstitial-free substrate. This generates high residual stresses and stacking faults (SFs) within the layer.

These effects, combined with the variegated treatment methods, make a comprehensive understanding of expanded austenite a complicated matter. During the last thirty years a number of research groups and industries have dedicated extensive studies on materials, processes, modelling and characterization methods. However, results are often controversial or only valid for specific cases.

1.2 Aim

In this study we characterize and compare the chemical and microstructural characteristics of expanded austenite formed through industrial plasma nitriding (PN) and gas carburizing processes on two austenitic stainless steels, 304L and 904L.

The aim of this project is to investigate the influence of the alloy composition and specific surface finishing as well as thermal annealing on the microstructure, phase constituents, strain evolution and hardening effect of expanded austenite by means of combined analysis techniques.

2 Materials and processes

2.1 Stainless steel

2.1.1 History

The most common carbon steels, on which the modern industry is largely based upon, generally exhibit poor resistance to environmental interaction. Rust is formed when steels are exposed to air. Corrosion becomes a significant issue especially in wet, marine and acid environments.

Although the beneficial effects of adding Cr as alloying element to common steel was recognised as early as the 19th century, it is only one hundred years later that the word *stainless* actually became part of the academic and industrial world.

The characteristic corrosion resistance of Cr-alloyed steels is given by the ability to form a thin, continuous, adherent, self-healing, stable and passivating native chromium-rich oxide layer. A steel can be considered *stainless* when containing at least ~11wt% Cr. However, it was early understood that Cr alone does not offer complete protection in every condition. In particular, addition of Ni and Mo are beneficial in Cl^--containing environment. These two elements not only modify the chemical composition of the passive oxide, but also change the phase constituents.

It was only after the Second World War and in particular after the ´70s that accurate control of C and N content during processing (argon-oxygen decarburization)[1] allowed maximum flexibility in alloy design without incurring significant technological issues (e.g. embrittlement during welding)[2].

The world of stainless steel (SS) is in constant expansion. In the last decades the world consumption has consistently increased by ~ 6%[3], as given in Fig. 1. Industries are striving to achieve better performances, while keeping an eye on costs and considering price fluctuations of key alloying elements.

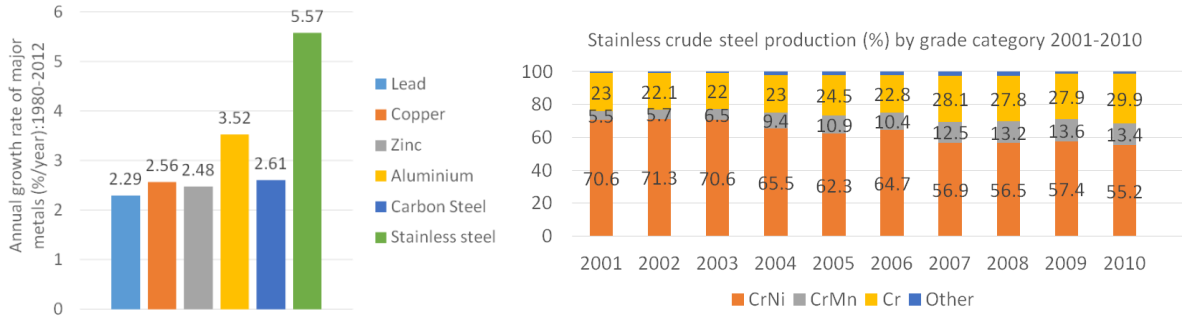

Figure 1 Left: the growth rate of major metals. Right: the stainless crude steel production by grade category. Redrawn from Stainless Steel in Figures 2013 – International Stainless Steel Forum[3].

2.1.2 Stainless steel grades

The family of SS can be divided into five different *types*: ferritic, martensitic, precipitation hardening, duplex and austenitic[4].

2.1.2.1 Ferritic grades

Standard ferritic grades contain mainly Cr (11 - 19%) as alloying element, with little or no Ni. This allows the cost connected to raw materials to be stable and low, comparable to that of carbon steels but with significantly improved corrosion resistance. Their microstructure is ferritic and they therefore are magnetic. To prevent the formation of Cr-rich carbides/nitrides at the grain boundaries during welding it is possible to add small amounts of Nb and/or Ti having higher affinity to C/N than Cr. As ferrite stabilizers, Nb and Ti can also be used to prevent formation of brittle martensite.

The field of application usually ranges from room to high temperature, especially in sulphur-containing atmospheres. Generally, ferritic stainless steels are not used at cryogenic temperature due to high brittleness in the low temperature range.

2.1.2.2 Martensitic grades

Martensitic grades contain similar amount of Cr to that of ferritic SS, but in order to increase the austenite stability range at high temperature, necessary for heat treatment, this requires addition of Ni, N or C. The martensitic stainless steels are magnetic and heat-treatable, following the same procedure as for conventional carbon steels (austenitizing, quenching, tempering). Stainless steels belonging to this grade are the least corrosion resistant and are normally employed in similar application fields as the corresponding martensitic steels, including surgical equipment, razors, cutlery, bearings, etc.

2.1.2.3 Precipitation hardening grades

Precipitation hardening stainless steel is a highly specialized class of materials, mainly used when higher strength at high temperature is desired, although the corrosion resistance is not superior to that of more conventional ferritic stainless alloys. They can be further classified as martensitic, austenitic or semi-austenitic, depending on the nature of the main constituting phase. Most precipitation hardening stainless steels contain Ti, Al, Cu, Nb and Mo for strengthening purposes.

2.1.2.4 Duplex grades

Duplex stainless steel grades have a multiphase microstructure, typically ferritic-austenitic. High Cr content (17 - 30%), with rather low Ni content (1 - 7%) produces almost equi-proportional balance of phases (ferrite and austenite) following heat-treatment in the two phase region. Other common alloying elements are Mo and N to improve strength, corrosion resistance against pitting and to balance the microstructure. Duplex stainless steels usually take advantage of both characteristics of ferritic and austenitic steels, with an additional advantage of the cost prospective thanks to the limited use of Ni.

2.1.2.5 Austenitic grades

Austenitic grades (ASS) comprise a large variety of stainless steels, mainly tailored to specific application requirements. The largest kind in terms of production and application flexibility is the Cr-Ni, also called “18 - 8” (type 304), with addition of Mo (type 316) for enhanced pitting resistance.

Being austenitic at room temperature thanks to the stabilizing effect of Ni (Mn, N as well in some cases), they exhibit high formability in the largest range of temperatures, from cryogenic to high temperatures, where the austenitic grades maintain their strength and formability more than ferritic grades do. The austenitic grades are not heat-treatable, but show excellent work-hardenability. Carbon lean variants have been developed (designated with L) to eliminate weldability problems related to carbides precipitation during welding, which lead to both embrittlement and loss of corrosion resistance.

Depending on the overall alloy composition and processing parameters, it is possible that a certain amount of δ-ferrite is retained within the austenitic structure[5], [6]. Moreover, several ASS alloys have tendency to form deformation induced martensite (α´), which has detrimental effect on corrosion resistance.

An empirical formula for determining deformation induced martensite formation temperature M_d was proposed by Angel and is related to the chemical composition as follows (eq. 1)[7].

$$M_d\left({}^{30}/_{50}\right)[°\mathrm{C}] = 413 - 13.7(\%Cr) - 9.5(\%Ni) - 8.1(\%Mn) - 18.5(\%Mo) - 9.2(\%Si) - 462(\%[C+N]) + \cdots \quad (1)$$

In the equation, $M_d(30/50)$ represents 50vol% of α´ martensite formed after a true tensile strain of 30%. Notice that the formula does not take into account factors such as strain rates and pre-existing stress conditions.

Austenitic grades are not free from limitations and drawbacks. The protective Cr-rich oxide tends to spall-off during heating cycles, due to the high thermal expansion coefficient difference between the oxide and the matrix[8]. Moreover ASS are susceptible to stress corrosion cracking[9]. In addition, as a consequence of the high work-hardenability, the ASS exhibit low fatigue endurance limit[10]. Furthermore, low surface hardness and poor wear resistance can be a limitation for many applications.

2.1.3 Effects of main alloying elements

2.1.3.1 Ferrite stabilizers

Chromium with a minimum concentration of 11wt% is the most important alloying element of stainless steels. The higher the Cr content, the higher is the corrosion resistance. This is also true for high temperature applications. As a strong ferrite stabilizer, Mo can significantly increase the strength at high temperature and the resistance to both general and pitting corrosion. However, the high cost and tendency to form unwanted secondary phases make Mo rarely exceed 6% in commercial alloys. When added in small amounts, Si increases resistance to oxidation. Titanium and Nb are strong ferrite and carbide formers. They act as “traps” for C and N, preventing Cr depletion.

2.1.3.2 Austenite stabilizers

Nickel is a main austenite stabilizing element. At least 8% Ni is necessary to assure an austenitic structure in ASS. Because of the relatively high cost and health-related concerns (allergies) there is a growing tendency to replace Ni with other austenite stabilizers. Manganese is used mainly to partly replace Ni in biomedical applications. Another austenite stabilizer, Cu, is able to increase corrosion resistance. It also increases N solubility and

improves hot ductility. Carbon is a strong austenite stabilizer and it increases the mechanical strength of the alloys. Although a relatively large amount is used in martensitic stainless steels, C is generally unwanted in other grades because it may combine with Cr to form carbides, lowering the corrosion resistance. Corrosion at grain boundaries can be a serious problem. In order to solve this, low-carbon bearing stainless steels are developed and classified as L, e.g. 304L and 316L. Nitrogen has the same effects as C. Both elements are interstitials and provide effective solid solution hardening effect. Nitrogen is more useful in this respect because it has lower tendency to cause intergranular corrosion. It is particularly beneficial for localised (pitting) corrosion resistance[11].

2.1.3.3 Nickel and chromium equivalents

Considering the high amount of alloying elements in SS, alloy design is of paramount importance. First of all, the composition of the alloy determines the chemistry of the native oxide formed at the surface, which is the key of corrosion resistance in SS. Secondly, each alloying element has either a ferrite or austenite stabilizing effect. The balance has significant impact on the final microstructure of the alloy which is in turn related to both corrosion and mechanical performances. The current available simulation tools are not always advanced enough to appropriately describe the coupling interaction between so many alloying elements; therefore empirical rules are still widely used. One of the most used is the Schaeffler-DeLong diagram (Fig. 2), which gives an empirical representation of austenite-ferrite phase stability by calculating "Ni-equivalents" and "Cr-equivalents" (eq. 2 and 3)[4].

$$Ni(eq) = \%Ni + 30 \times \%C + 0.5 \times \%Mn \quad (2)$$

$$Cr(eq) = \%Cr + \%Mo + 1.5 \times \%Si + 0.5 \times \%Nb \quad (3)$$

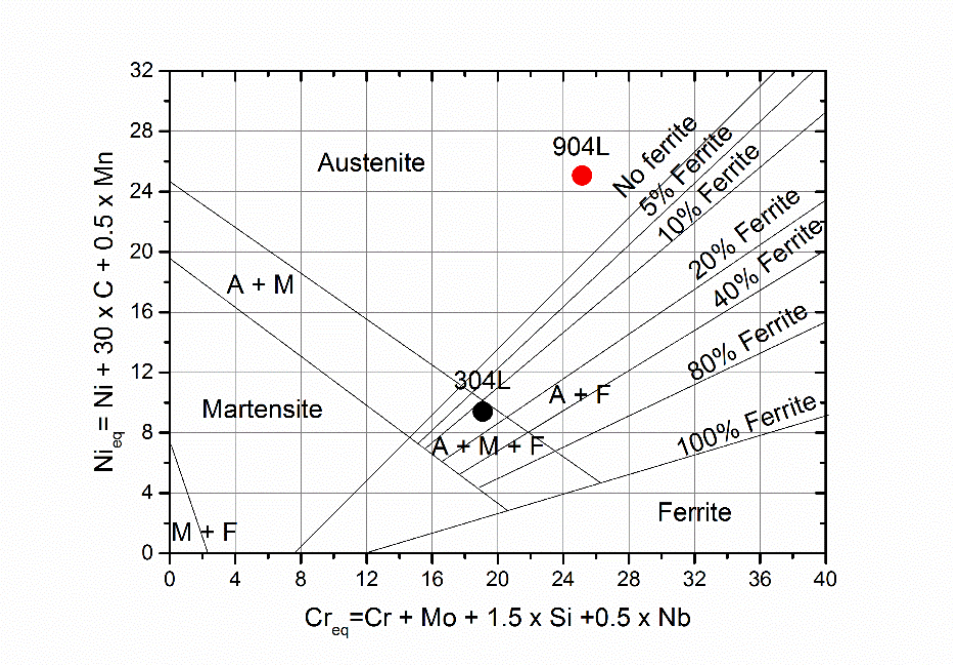

Figure 2 Schaeffler diagram with 304L and 904L equivalent Ni and Cr composition, redrawn from reference (A: austenite; F: ferrite and M: martensite).

This is the most convenient way to represent the effect of various elements on the microstructure of Cr-Ni stainless steels. It can be seen from Fig. 2 that the high alloyed 904L

is within single austenite region while the 304L may contain small amount of ferrite and even possibly some martensite. Several empirical diagrams can be found in literature, each with varied application ranges and equivalence coefficients. They are routine references for studies on casting and welding. However, such empirical rules should not be taken as golden rules, since they do not take into consideration some important factors, for example cooling rates.

2.1.4 Surface finishing

Surface finishing is an important operation during production of SS. It is generally accepted that limited maintenance is required for SS products through the whole life cycle. Therefore the surface finishing is usually carefully chosen by the customer and is likely to be the one for the final product.

Pickling is the routine process for removing the oxide scales formed during annealing, hot-forming and joining operations. This oxide scale differs from the protective passive film typical of SS. It is instead a thick crust of mixed oxides formed during complex thermal cycles in non-controlled atmospheres. Below the oxide scale there is usually a Cr-depleted layer that needs to be removed in order to guarantee self-repairing capabilities of the desired oxide layer. Pickling solutions usually include HNO_3, H_2SO_4 and HF. The use of HCl should be avoided since it might lead to localised pitting corrosion. When the oxide scale is too thick and exhibits high chemical resistance, for example in case of high alloyed SS, the pickling phase is preceded by a mechanical descaling such as shot-peening, sandblasting or brushing[4].

Depending on the desired level of roughness fine grinding, polishing or electro-polishing can be applied. High reflectivity, which is directly related to roughness, is often desired by final users[12].

2.2 Materials in this study

This thesis focuses on two austenitic stainless steel grades, 304L and 904L, which can be considered as the extremes in terms of corrosion resistance and cost. Both are low-carbon steels containing less than 0.03 wt% C, which is particularly important in order to minimize the risk of intergranular corrosion successive to welding operations. Nominal chemical compositions as reported by Avesta Research Centre are shown in Table 1. Both materials used in this study were supplied by Outokumpu Stainless AB (Sweden) in form of 3 mm thick plate.

Table 1 Nominal composition of 304L and 904L austenitic stainless steels (wt%).

	Fe	C	Mn	Cr	Ni	Mo	Si	S	P	N	Cu	Ti
304L	Bal.	0.019	1.63	18.25	8.05	0.43	0.28	0.001	0.028	0.072	0.33	0
904L	Bal.	0.011	1.62	20.3	24.26	4.37	0.33	0.001	0.023	0.054	1.41	0.007

2.2.1 304L austenitic stainless steel

Type 304L stainless steel, also known as ASTM/AISI/SAE 304L, UNS S30403, A2 stainless steel or EN 1.4307, is the most versatile and widely used steel available in the market. It is an "all purpose" grade characterized by good corrosion resistance, excellent formability and weldability. Additionally it is among the cheapest grades of stainless steels, making it the favourite choice of industry. It is particularly suitable for large structures such as food and

beverages containers, pharmaceutical industry, kitchenware, construction material (screws, bolts, etc) as well as for exhaust systems within automotive industry[13].

As other ASS, 304L is non-magnetic, even though some δ-ferrite (0-5%) is commonly found in the form of stringers[14]. Controversial results have been reported regarding the effects of δ-ferrite, including resistance to stress-corrosion cracking and tendency to cracking during cold work[15],[16]. Applying Angel's equation, it infers that deformation induced martensite can form at room temperature in 304L. This was experimentally demonstrated by several researchers in a number of experiments including uniaxial tensile tests and cold working[7],[19],[20]. In our studies we also observed the formation of deformation induced martensite due to mechanical polishing through XRD and EBSD measurements, as shown in Fig. 3.

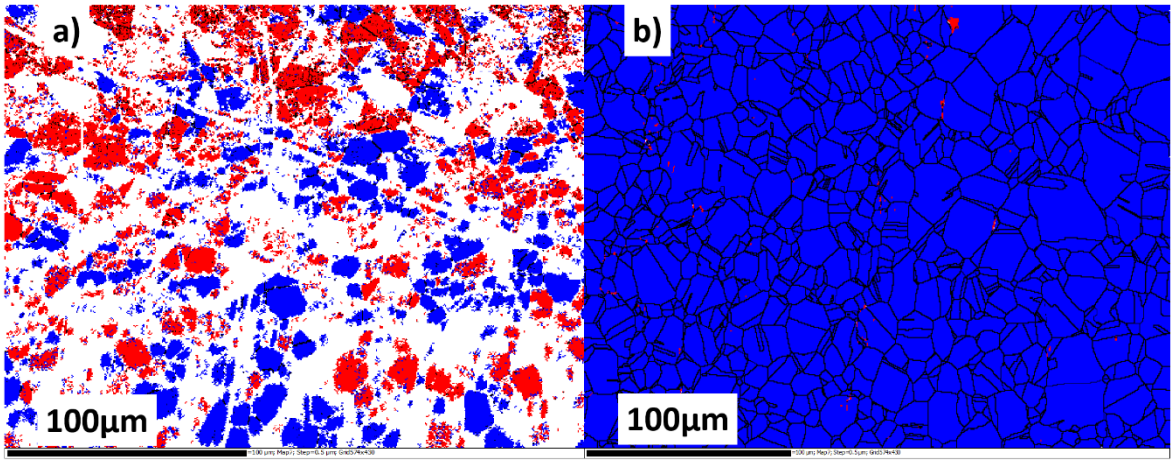

Figure 3 Left: Deformation induced martensite (red) on mechanically polished 304L surface. Right: ferrite stringers (red) in electropolished 304L surface (figure from Paper III).

2.2.2 904L austenitic stainless steel

Type 904L, also known as UNS N08904, ASTM/AISI 904L, EN 1.4539, is a high-alloy austenitic stainless steel. It is often referred to as "superaustenitic" owing to the high stability of the austenitic phase (cf. Schaeffler diagram in Fig. 2) and high corrosion resistance. Alloy 904L is not susceptible to deformation induced martensite formation at room temperature, as suggested by Angel's equation.

The large amount of expensive alloying elements, especially Ni and Mo, make this material suitable only for high performance applications, where superior corrosion resistance is required and cost is not a key issue[19]. The alloying element Cu also offers a decisive improvement on corrosion resistance in specific environments that contain sulphuric acids and reducing agents. In particular, 904L is designed for applications involving concentrated acid solutions and Cl^--containing environments, especially at relatively high temperature, where conventional ASS such as 304L would fail[20]. Therefore, 904L is mainly employed in processing plants such as pulp and paper industry, for oil and gas applications, and in marine environment.

2.2.3 Hardening mechanisms in austenitic stainless steel

The major weaknesses of austenitic stainless steels are their low surface hardness and unsatisfactory tribological behaviour. It is a common interest in research and industry to improve these properties in order to extend the fields of application and to increase the lifetime of components made of these materials, making them more viable and cost effective materials choices.

General hardening mechanisms in metals include work hardening, solid solution hardening, grain refinement, transformation hardening and precipitation hardening. While the final component often shows a hardening effect which is a combination of several mechanisms, the routes and contributions vary significantly depending on the materials and applied hardening treatment.

As shown in previous sections, fully austenitic SS cannot be heat-treated to achieve an effective hardening through martensite formation. It is also not recommended to induce precipitation hardening through formation of Cr-compounds since that would compromise the general corrosion resistance. When alloying elements having higher affinity with interstitials are added, selective precipitation without Cr depletion occurs. We then enter in another class of SS, precipitation hardening stainless steels.

Cold-working can be a viable solution for hardening through deformation, given the high work-hardenability of ASS. However, these types of treatments (cold-rolling, sandblasting, shot peening) have complex effects on microstructure and corrosion resistance[21],[22]. Furthermore when metastable ASS such as 304L are subjected to severe mechanical deformation, martensitic transformation may occur, decreasing the general corrosion resistance[23]. On the other hand, subsequent controlled annealing procedure followed by quenching might induce sufficient grain refinement by recrystallization to actually improve both tribological properties and the general corrosion resistance thanks to the increased diffusivity of Cr through the grain boundaries created during the process[24].

When talking about solid solution hardening, one has to distinguish between substitutional solid solution and interstitial solid solution hardening. The first is caused by the different size of atoms constituting the alloy which induces a lattice strain field, hindering dislocation movement. This is normally present in ASS given the significant amount of alloying elements within the austenitic matrix. In the second case, lattice strain is induced through occupancy of interstitial sites by usually N and/or C (but also B sometimes). We have already mentioned that in ASS interstitial content is usually kept as low as possible during production to avoid Cr-precipitates. For the same reason, conventional high temperature ($T > 500°C$) thermochemical treatments such as nitriding, carburizing and carbonitriding aiming at introducing large amounts of interstitials are not suitable, since they generally lead to sensitization of grain boundaries (Fig. 4)[25],[26].

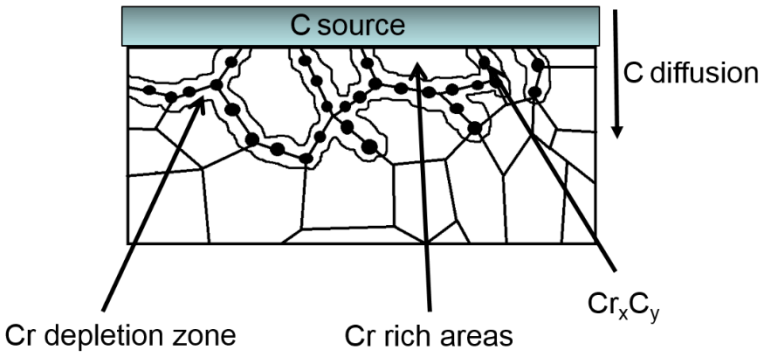

Figure 4 Schematic of sensitization process following traditional high-temperature carburization process. Cr-rich precipitates formation at the grain boundaries lead to Cr depletion in neighbouring regions leading to intergranular corrosion.

2.3 Low-temperature thermochemical treatments

Developing efficient and industrially scalable surface hardening processes for austenitic stainless steels without hindering the corrosion resistance is highly desirable but poses significant technological challenges. Since the middle of the 80s, thermochemical treatments involving diffusion of C and/or N at low temperature (T < 450°C) provided new possibilities.

It was observed that precipitation of Cr compounds could be delayed, allowing sufficient interstitial diffusion to form a hardened layer having thickness of several μm. At such low temperatures, the interstitials not only remain in solid solution, but they can also reach concentrations orders of magnitude higher than thermodynamic equilibrium. This phenomenon is called "colossal supersaturation" and leads to the formation of a "metastable interstitially supersaturated expanded austenite", simply referred to as "expanded austenite" or "S-phase".

The most common methods for LTTT are nitriding and carburizing, or combinations of the two, both in gas or plasma processes.

Gas processes have the advantage of being highly controllable (gas composition, process parameters) and parameters can be adjusted from "traditional" heat treatment processes. However, one of the downsides is the difficulty to induce interstitial diffusion through the protective oxide film of austenitic stainless steel. A specific reduction pre-treatment is typically necessary, which increases cost and makes the process more complicated.

Plasma processes, however, work at lower pressures and the total gas consumption is therefore significantly reduced, with both economic and environmental benefits. Another advantage is the possibility to use non-hazardous N or C-carrying gases, since an efficient activation process is able to take place under the action of plasma. Moreover, the passive layer is removed in-situ by the constant sputtering process at the material surface. However, plasma techniques suffer from the high costs related to the pumping system necessary to reach good pre-vacuum and the requirement for optimizing and controlling many parameters. Moreover, depending on the geometry of the part to be treated and the plasma techniques, inhomogeneity problems can arise due to charging effects, arcing or shadowing.

In this study we have characterized the expanded austenite layer formed by means of two industrial processes, plasma nitriding and gas carburizing, performed by Bodycote Värmebehandling in Stockholm and in Vellinge (Sweden).

2.3.1 Nitriding

2.3.1.1 In general

Nitriding is a conventional surface engineering method which relies on nitride formation within a metal matrix. Among the various thermochemical treatments it is the one requiring the lowest temperature (from 315°C to 540°C)[27]. Alloys containing significant amount of nitride formers such as Al, Cr, Ti, Mo are also called "nitriding alloys" and are specifically designed to benefit from such processes.

The typical structure of a nitrided layer includes a gradient of nitride compounds with decreasing stoichiometry, followed by an interstitial diffusion layer and finally the bulk, as shown in Fig. 5.

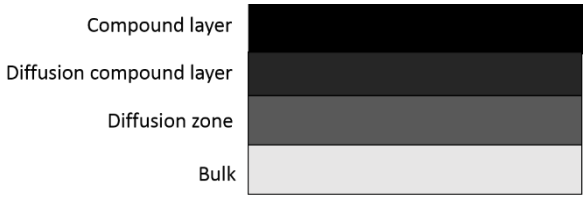

Figure 5 Schematic structure of a nitrided layer.

The composition and proportion of the compounds present within the layer is highly dependent on both the process parameters and the alloy composition (ε-$Fe_{3-2}N$, γ´-Fe_4N, CrN in stainless steel). Higher temperatures and longer treatment times lead to an increase in thickness of the compound layer, while more alloyed steels show a thinner layer compared to low alloyed steels[27].

Nitriding of austenitic stainless steel is mainly performed either through gas nitriding or plasma nitriding.

Gas nitriding relies on the use of ammonia or ammonia-hydrogen mixtures (eq. 4)[28], but first it requires removal of the protective oxide layer. This can be performed *ex situ* by electrochemical treatment of the steel, which leads to dissolution of the Cr-rich oxide and subsequent plating of a thin Ni or Fe layer to prevent re-passivation[29]. Nickel and Fe also act as catalysts for the decomposition reaction of ammonia during the heat treatment[30].

$$NH_3 \rightarrow [N] + 3/2H_2 \qquad (4)$$

After the atomic nitrogen diffusion, the catalyst layer is successively removed by acid and passivation can be restored. One advantage of this method is the possibility to store oxide stripped components before heat treatment. Moreover, the compound layer formed during nitriding can easily be removed in the post-treatment process using acids. The disadvantage resides in the number of steps required in this procedure.

Alternatively, de-passivation can be performed *in situ*, within the heat-treatment furnace. The procedure involves flushing with halogen-based compounds (e.g. HCl, NF_3) prior to nitriding

process. However, these compounds are aggressive to the furnace. Addition of NO to NH_3 has been proven to be a possible alternative for activation of SS surfaces[31].

2.3.1.2 Plasma nitriding in this study

In PN, the part to be treated is placed within the vacuum chamber, which is evacuated until suitable vacuum condition is reached (depending on the specific plasma technique).

In a generic DC plasma set-up (Fig. 6), a mixture of N_2/H_2 is introduced into the chamber and kept at a pressure in the order of several tens mbar. Subsequently a DC voltage in the range of 100-1500 eV is applied between a cathode and the part at anodic potential, generating a glow discharge. At this point, the positively charged species are accelerated towards the part to be treated and impinge, converting their kinetic energy into heat and sputtering atoms from the sample surface. In this way a layer with high N concentration is created in the near-surface zone of the sample and diffusion can start. External heating and temperature monitoring are usually required to assure a fast and controlled obtainment of desired operating temperature[32].

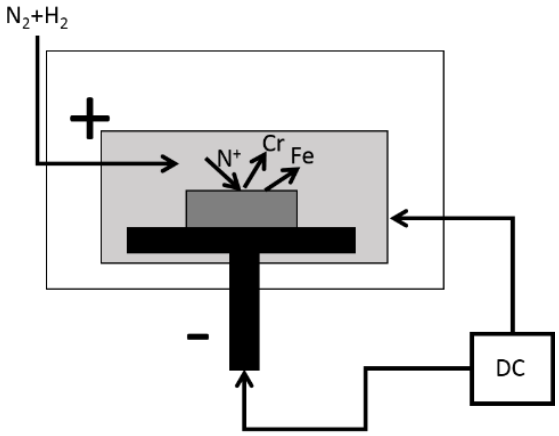

Figure 6 Schematic arrangement of plasma nitriding process.

In this study, PN of two austenitic stainless steels 304L and 904L was performed in industrial furnaces at 400°C in N_2/H_2 atmosphere. Two process conditions were used, i.e., at low N_2 partial pressure (L, p_{N2}=6%) for 24 hours and at high N_2 partial pressure (H, p_{N2}=25%) for 99 hours, respectively. Details about other process parameters such as surface activation conditions, total pressure and specific plasma technology used are proprietary and their influence on the nitrided layer microstructure is not within the scope of this study.

As seen in Fig. 7e, the PN process might result in a non-homogeneous treatment of the coupons. The central area exhibited a dull appearance (Area 1), while the rest of the coupon remained mirror-like (Area 2). Occasionally, bright regions could be observed near the edges of the coupon. This effect is probably related to the specific geometry of the PN employed and due to edge effects on the samples.

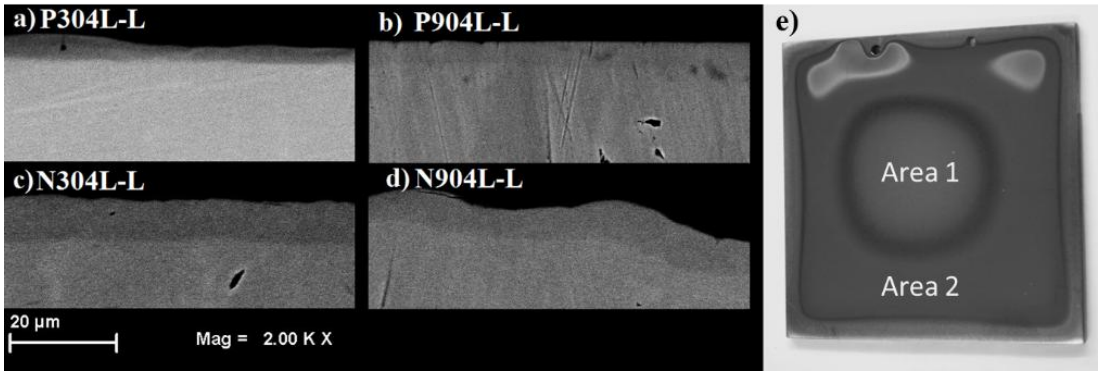

Figure 7 a) (a–d) Backscattered electrons image of the cross section from nitrided steels and e) top view of the polished and nitride P904L-L (Paper I).

2.3.2 Carburizing

2.3.2.1 In general

Carburizing is a very old process, used for centuries to perform surface hardening of steels. Powder carburizing (charcoal), salt bath carburizing (cyanides), gas carburizing and plasma carburizing are among possible carburizing techniques available nowadays. However, only gas and plasma methods are viable options for ASS thanks to their lower working temperature requirements.

Gas carburizing methods are the most widespread and consolidated techniques for surface hardening of SS. Halogen reduction of surface oxide layer using the so called "endothermic gas" mixture of $CO/H_2/H_2O$ is a standard procedure in conventional carburizing treatments, as indicated in Fig. 8[33].

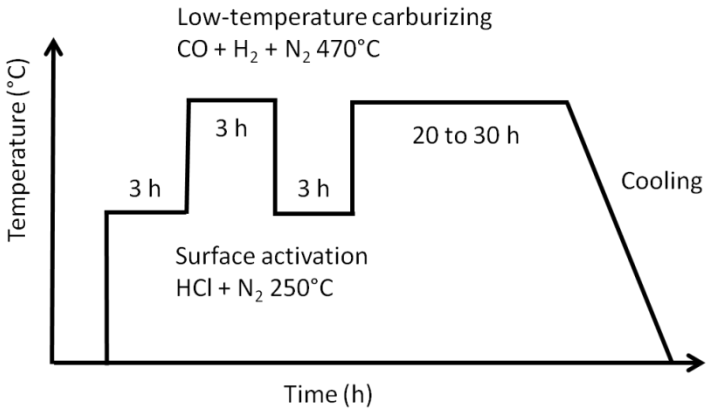

Figure 8 Schematic process of Swagelok low-temperature carburizing treatment[33].

More modern techniques use gas mixtures which are able to both reduce the passive layer and induce an efficient precipitate-free carburizing layer at the same time. The recently patented processes by Swagelok Company and Expanite A/S, for example, include acetylene/hydrogen and acetone among other gases[34][35].

The studies on low-temperature plasma carburizing started in the ´90s and continued through the ´00s. They are particularly interesting in an industrial prospect since this process allows for higher efficiencies, while using inexpensive carbon carrying gases (e.g. CH_4, C_3H_8) otherwise impossible to thermally decompose in traditional gas carburizing. Hydrogen is

added to limit the formation of soot, often formed in low-temperature carburizing (LTC) furnaces and on treated parts. Unfortunately, given the high industrial interest, important process parameters (temperature regimes, gas mixtures) involved in successful surface hardening of stainless steels through PN are often kept as trade secrets.

2.3.2.2 Gas carburizing in this work: Kolsterising®

In this study, the surface modification induced by Kolsterising® K22 LTC treatment supplied by Bodycote Värmebehandling was characterized. This treatment was first presented by Kolster in 1983 with the name HardCorr, and can be considered as the first LTC process ever entering the market[29]. Unfortunately key process parameters such as gas composition, time-temperature regimes and surface activation procedures have not been published.

It is claimed that this process induces C supersaturation within several austenitic stainless steel grades, including 304L and 904L, with no Cr-containing precipitates[36]. A diffusion layer having thickness between 20µm and 30µm is commonly reported, with surface hardness values as high as 1200 HV[33].

3 Expanded austenite

Throughout this thesis and in all the appended papers, “S-phase” and “expanded austenite” are used interchangeably to describe a metastable supersaturated interstitial solid solution of N or C in an austenitic matrix.

3.1 History

It is generally accepted that S-phase was first discovered in 1985. Beneficial effects of interstitial supersaturation in austenitic stainless steels were demonstrated by independent studies made by Zhang and Bell, at Birmingham University[37], and Ichii from Kansai University[38]. Dedicated works were performed by both groups on PN, a prospective technology for surface hardening of stainless steel while avoiding Cr nitrides precipitation. The characteristic presence of a white-etching layer was the first hint of maintained, or even improved corrosion resistance of the hardened layer.

The first term used when addressing the hardened layer was “S-phase”, referring to the “satellite” peaks appearing at lower angles of the typical X-ray diffraction patterns of the FCC phase from the austenitic substrate (Fig. 9)[39].

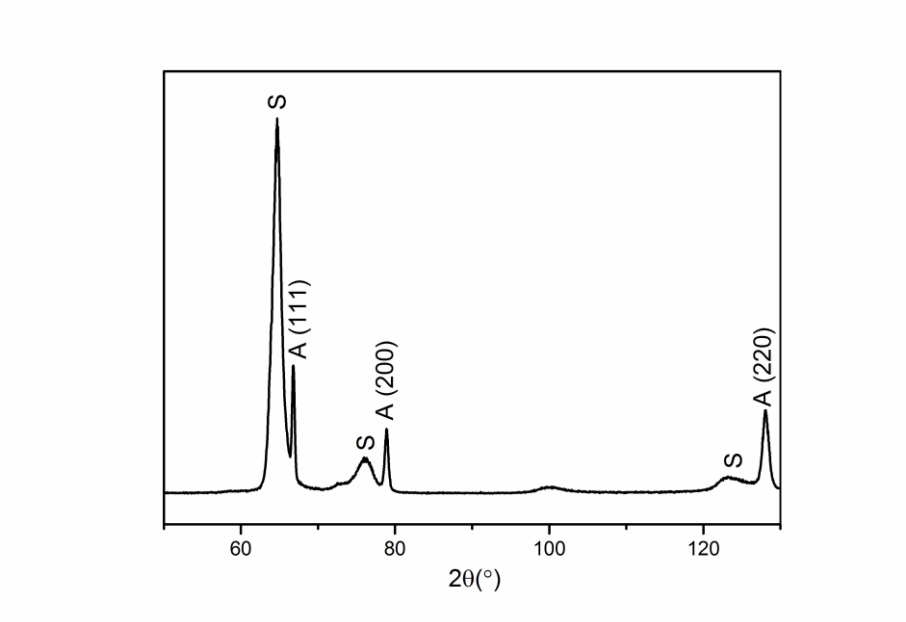

Figure 9 S-phase as identified from data collected by the author on plasma nitrided 904L (Paper I).

In fact, two years before Zhang, Bell and Ichii, Kolster had already published results of a surface treatment which provided outstanding hardening effect to stainless steels, and began commercialization of a low-temperature carburizing process named HardCorr. It was later renamed Kolsterising and it is the property of Bodycote Heat Treatments[40]. Kolster did not initially disclose the type of treatment involved and process details are still a major industrial secret[40].

It has been speculated that studies performed during the ´60s on liquid sodium induced corrosion by Litton, Morris, Anderson and Sneesby on stainless steel were the source of inspiration for Kolster[40]. In those studies, carbon contaminations in liquid sodium were causing carburization of stainless steel and loss of corrosion resistance. It was however

observed that an interstitial diffusion zone with high corrosion resistance was present at exposure temperatures of below 550°C[40].

3.2 Microstructure and characteristics

3.2.1 Crystal structure

The nature of nitrogen/carbon induced S-phase has been disputed for many years and several denominations were used to describe what is nowadays most commonly referred to as expanded austenite. This was due to the difficulty in determining the "real" crystal structure of interstitially supersaturated austenite.

Nitrogen containing S-phase was initially described by Ichii, Zhang and Bell as a mixture of γ´ compound M[Cr, Fe, Ni]$_4$N having FCC structure and austenite. It was however found that lattice expansion measured by XRD was not isotropic, being more pronounced from (200) diffraction peaks; therefore some authors believed that expanded austenite has a tetragonal nature and referred to it as ε´ or M-phase (from "martensite"). Some other authors have even considered an amorphous nature[39].

As demonstrated by Fewell et al. using TEM studies, the nature of expanded austenite can be described as a "substantially" cubic FCC structure[41]. The presence of a thin compound layer consisting of CrN and α-Fe is frequently encountered in PN, but it seems to be an effect of the specific treatment, and can be thinned or eliminated with appropriate N_2-H_2 gas mixing.

There is still debate about the origin of the anomalous expansion measured by XRD; three of the most commonly accepted explanations are as follows.

1) Tetragonal deformation would be the simplest explanation of the XRD patterns, and corroborated by the studies of Martinavicius and Abrasonis on single crystal which confirms the enhanced diffusion in direction perpendicular to {100} crystal orientations[42][43][44]. This implies that different grains having anisotropic expansion is possibly due to different stress relaxation at the surface. This theory was recently further strengthened by EBSD analysis conducted by Templier et al.[44] who showed the existence of a texture gradient through the expanded austenite layer.
2) Alternatively, Fewell et al. proposed a triclinic type of distortion. However fundamental complementary diffraction lines (e.g. (100), (221)) have not been detected yet[45].
3) A third theory, proposed among others by Christiansen and Somers, ascribes the (hkl)-peak shift to the presence of SFs induced by nitriding process and consequent nitrogen supersaturation[46]. The importance of SFs is generally accepted and a high amount of twins and SFs is observed by TEM analysis[45].

The same description can be applied to C-stabilised expanded austenite, with the difference that a surface compound layer is rarely observed. However, presence of χ-Hägg (M_5C_2) carbides was observed by Farrell et al. for LTC of 316L with Kolsterising treatment[47] and the same was observed for 304L by the author (Papers II and III).

3.2.2 Supersaturation, stacking faults and residual stresses

Solid solubility of C in austenitic stainless steels like AISI 304 or 316 is normally in the order of maximum 0.015at%, while in expanded austenite up to 14at% was reported in literature

and confirmed by the author in our Paper III. Metastable solubility of N is even higher and can reach values as high as 25at%, while thermodynamic equilibrium is at < 0.65% N[39].

At least two reasons can be counted as important for the higher solubility threshold of N compared to C. First of all N has smaller atomic radius than C, which allows to fill octahedral interstitial sites of austenite with a comparably smaller lattice distortion. Another reason is the higher affinity between N and nitride forming elements (mainly Cr in stainless steels) compared to C for carbides. It has also been shown that presence of strong nitride/carbide formers (in order Ti, V, Nb, Al, Cr, Mo, Mn) can significantly enhance solubility of interstitials in ASS, while Ni and Si hinder it[48].

The short range ordering between N and Cr was proven by Oddershede et al. with extended x-ray absorption fine structure (EXAFS), revealing a different interaction compared to that of a CrN-type of precipitates[49]. A similar study performed on C-containing S-phase showed a smaller ordering compared to N[50].

A linear dependence between austenite lattice parameter (a) and interstitial content was proven by Christiansen and Hummelshøj for both nitrogen stabilised (γ_N)[51] and carbon stabilised (γ_C) expanded austenite (interstitial lattice expansion coefficient is expressed in nm), as shown in eqs. 5 and 6[52]:

$$a = a_0 + 0.05987\, y_N \qquad (5)$$

$$a = a_0 + 0.06029\, y_C \qquad (6)$$

Here, y_N and y_C are octahedral interstitial occupancies of N and C respectively, or in other words, the number of interstitial atoms per one hundred metal atoms. It has to be highlighted that the study by Christiansen and Hummelshøj was performed on highly controlled nitriding/carburizing conditions, assuring homogeneous interstitial content throughout the whole metal thin foil used as a substrate, therefore eliminating concentration and stress gradients.

Except for thin foils (< 100 μm), through-specimen homogeneous carburization can never be achieved and the lattice expansion is confined by the bulk. The gradient in interstitial concentration arising from diffusional processes causes a gradient in compressive residual stresses through the expanded austenite layer. Below the interstitially enriched zone there will be a tensile residual stress state, as schematically shown in Fig. 10. Therefore very high compressive residual stresses (> 2 GPa) arise in a region below the surface[53].

Strains are directly related to stresses through direction dependent elastic constants (also called X-ray elastic constants). For this reason, X-ray diffraction patterns of expanded austenite, representing diffraction planes having a gradient in spacing, are often significantly broadened when compared to original material.

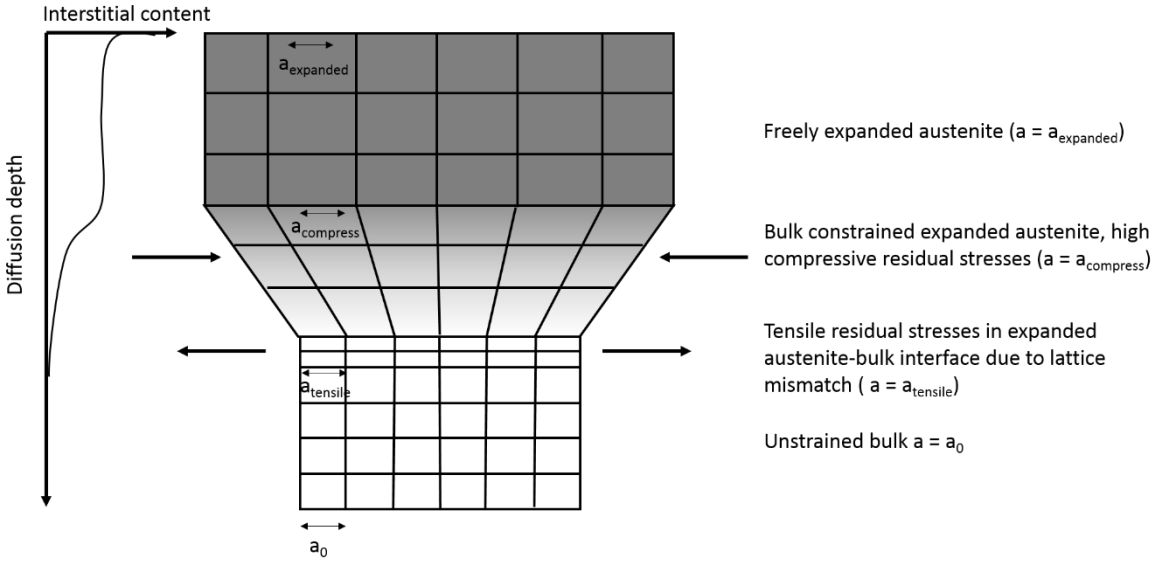

Figure 10 Schematic lattice stress-strain state induced by expanded austenite formation (not in scale).

High residual stresses are usually, at least partly released by plastic deformation. In case of expanded austenite there is commonly observed presence of slip bands and even twinning, as indicated in Fig. 11.

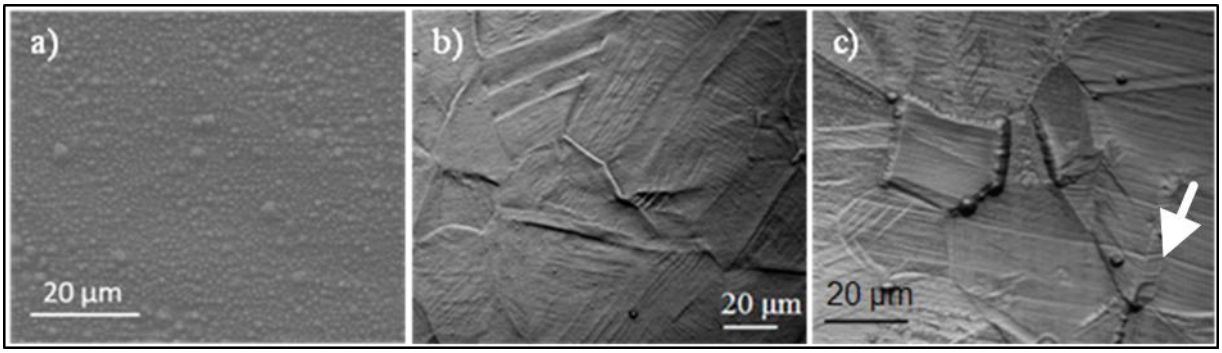

Figure 11 Topography of plasma nitrided (a) P304L-H, (b) P304L-L and (c) P904L-H. Plastic deformation in the form of slip bands and twinning is evident, in particular in 904L. Different protrusion of grains is also observed (Paper I).

In particular, twins are related to the SF probability and influence both XRD peaks shape and position[54]. The effect of alloying elements in a complex ASS is not completely understood, but it is believed that N in LTN materials lower significantly the SF energy, thus promoting twinning[55].

3.3 Interstitial diffusion mechanisms

A precipitate free interstitially supersaturated case can only be formed if the diffusivity of interstitials at a certain temperature is significantly higher than the diffusivity of reactive substitutional elements, such as Cr for ASS. This is generally true for temperatures below ~ 450°C, where C and N diffusion coefficients are several orders of magnitude higher than Cr.

One of the most interesting characteristics of expanded austenite is the exceptionally high diffusion rate of interstitials. Using a classical diffusion model, Williamson found that the theoretical activation energy for N interstitial diffusion (1.45 eV) in expanded austenite is significantly lower than the one reported for this diffusion in FCC phase in SS (1.87 eV) and

in Fe (1.74 eV), explaining why interstitials diffuse four to five order of magnitude faster through expanded austenite compared to austenite in ASS[56].

However, the interstitial concentration profiles cannot be correctly predicted by Fick's second law. A "trapping" mechanism was instead proposed by some researchers who hypothesized the role of Cr as imposing octahedral "trap sites", which are progressively saturated before further diffusion is allowed[57]. With this model we can explain the observed constant concentration plateau. A subsequent "detrapping" contribution in the model is particularly useful when describing contemporary or sequential C and N diffusion[58]. C is replaced by N in the traps thanks to the higher interaction between N and Cr, with carbon being "pushed-in", generating a double expanded austenite layer. This also explains why LTN materials present a more steep diffusion profile after the concentration plateau region compared to that when introducing C. For the same reason, the γ_N is generally thinner than γ_C for comparable time-temperature regimes. Moller and Parascandola presented a model of interstitial concentration dependence on depth and time *c(x, t)* for ion implantation plasma nitriding, where interstitial concentration in solute form $c_s(x, t)$ and trapped form $c_T(x, t)$ contribute separately, see eq. 7 below[59].

$$c(x,\ t) = c_s(x,\ t) + c_T(x,\ t) \qquad (7)$$

$$\frac{\partial c_s}{\partial t} = D\frac{\partial^2 c_s}{\partial x^2} + j_0 f_R(x) - T(x,t) \qquad (8)$$

Equation 8 gives the diffusion equation of interstitial solute. The first term on the right is the contribution of classical concentration gradient diffusion ($D\frac{\partial^2 c_s}{\partial x^2}$). The second term is the incoming flux of ions $j_0 f_R(x)$ and $T(x,t)$ represents the amount of trapping as expressed in eq. 9. This trapping contribution is dependent on the trap radius (R_T), the trap concentration (c_T), the binding energy of the traps (U_T), the coordination number (n_z) and the host atomic density (n_H).

$$T\ (x,\ t) = 4\,\pi D R_T \left[c_s(c_T - c_t) - z n_H c_t e^{-\frac{U_T}{kT}}\right] \qquad (9)$$

The diffusivity is not only dependent on the concentration gradient but also on the concentration itself[60]. Diffusivity is higher at high concentrations, probably due to the lattice expansion which further reduces diffusion activation energy. When interstitial content is above a certain threshold (e.g. y_N= ~ 0.45 for 304 and 316) diffusivity decreases again, probably due to an "over-saturation" of interstitial sites, reducing probability of inter-interstitial sites jumps[60].

Original lattice parameter of an ASS alloy seems to have significant influence on the solubility and diffusion properties within S-phase[61]. It was shown and confirmed that large alloying elements such as Mo and Cu can enhance diffusion and possibly contribute to increase the supersaturation limit (Paper III) [62][63].

Alloy composition is not the only determining factor in diffusivity of interstitial species in forming an expanded austenite layer. It was reported that externally applied tensile stresses can positively enhance the final case thickness[64]. The same is true for high plastic deformation or grain refinement, which can provide low-energy diffusion paths through grain boundaries and high dislocation density regions[65].

Presence of ferritic/martensitic phases can significantly delay the growth of S-phase[39]. Consequently, precipitates might instead be formed.

3.4 Thermal stability

Expanded austenite is inherently metastable, with thermodynamic driving force to form CrN precipitates in case of γ_N and Cr_xC_y for γ_C.

It has been observed that prolonged treatment times of LTTT can lead to unwanted Cr compound precipitation. For nitriding of stainless steels, precipitation of CrN and Fe_xN compounds is commonly reported[66][67][68]; while for carburizing processes precipitation of M_5C_2 (monoclinic χ-Hägg carbides) may occur[49],[71].

Kinetic of thermal decomposition of expanded austenite, leading to massive Cr depletion and loss of ASS corrosion resistance, is of paramount importance for industrial application. Several studies about thermal decomposition of most common ASS alloys, e.g., AISI 316L and 304L have been published. Li et al.[70][39] claimed the maximum temperature is about ~ 500°C for γ_N and ~ 650°C for γ_C S-phase before rapid decomposition (< 1 h) occurs. However, much lower operating temperatures are admissible in real applications. Bodycote recommends that it should not exceed ~300°C for materials treated with Kolsterising treatment, while laboratory tests on AISI 316L shows that isothermal decomposition occurs at ~ 300°C for γ_N and ~ 350°C for γ_C, giving a few years lifetime to expanded austenite[70], [71],[72].

Experiments on isochronal annealing (heating rate 0.417°C/s) by Christiansen on N-supersaturated 304L and 316L demonstrated that alloy composition has an influence on decomposition temperature and route. Decomposition of AISI 316L takes place at temperature about 50°C higher compared to 304L[73]. When annealing is performed in a reducing atmosphere, denitriding is observed and is more prominent in 316L. The reason is (supposed to be) the presence of Si in 304L, which might form silicon nitrides and "trap" more nitrogen within the material. Further analysis also proved that 304L and 316L decompose with formation of different products, consequently suggesting different decomposition routes. Expanded austenite in 304L evolves through a eutectoid decomposition route (eq. 10), leading to ferrite and nitrides precipitation. A discontinuous process is instead hypothesised for 316L, where the nitrides are accompanied by austenite phase (eq. 11[73]).

$$\gamma_N \rightarrow \alpha + CrN \qquad (10)$$

$$\gamma_N \rightarrow \gamma + CrN \qquad (11)$$

The presence of Mo might influence the decomposition route by shifting the ferrite-austenite transformation temperature, giving rise to larger range of stable austenite in 316L[73].

Thermodynamic calculations suggest that the stability of precipitate species in carburized ASS is highly dependent on the carbon supersaturation levels. The higher the carbon content, the higher the "order" of the carbide ($M_3C_2 > M_7C_3 > M_{23}C_6$)[40].

3.5 Mechanical, tribological and corrosion properties

3.5.1 Mechanical properties

One of the main characteristics of expanded austenite is the extremely high surface hardness, even higher than that of hardenable martensitic stainless steels. It is not unusual to achieve hardness level of above 1000 HV, with γ_C having average surface hardness of 800-1000 HV and γ_N showing values of 1200-1500 HV. The generic explanation of this hardening is the presence of high amount of interstitials, accounting for solid solution hardening and tetragonal lattice distortion due to the strain field created in the material. Larger effects on hardness are normally achieved by LTN treatments. This can easily be related to the higher interstitial occupancy and consequently higher residual stresses.

It is important to remember that measured hardness values on materials subjected to LTTT are extremely dependent on the applied loads. Expanded austenite is usually rather thin (few tens of μm) and with a hardness gradient throughout the bulk. Hardness measurements performed perpendicularly to the case-hardened surface will show high hardness enhancement at low loads and low surface enhancement at high loads. Moreover, microhardness measurements performed on cross-sections systematically give lower hardness values than surface measurements performed with the same load.

Another important property to be taken into consideration is toughness. From micro-tensile test it was observed that γ_N significantly reduced the ductility of the base material, while γ_C does not show reduction. Hardness and toughness are often competing properties. The higher dislocation density and more twins induced in γ_N are likely to be responsible for this "nitrogen embrittlement".

Fatigue resistance is also considerably improved (~ 20 - 50%) both by LTN and LTC, thanks to high hardness and compressive stresses. It was observed that failure cracks develop mainly at the interface between expanded austenite and bulk material.

3.5.2 Tribological properties

Improvement of tribological properties in ASS is one of the main driving forces for understanding and optimising expanded austenite. Similar to hardness, wear measurements are highly dependent on the method. For low applied loads in the order of ~10 N, a reduced wear rate of even two orders of magnitude is reported and it is generally accepted that expanded austenite provides consistent wear resistance[74],[75].

When high loads are applied, however, the so called "thin ice" phenomenon might occur and wear resistance might actually be reduced. Due to the relatively small thickness of expanded austenite layer, then when the applied load is too high the stresses are concentrated in the bulk region and a "ploughing" effect can be observed, causing the loss of the hard layer[76].

The same problem arises in terms of load bearing capacity. When applied loads are high enough to be concentrated in proximity of the case-bulk interface, cracking can occur there[76]. This can be an issue for applications such as bearings or joints under compressive stresses.

3.5.3 Corrosion properties

Precipitate free expanded austenite conventionally appears on metallographic cross sections as white etching layer. This suggests that wet corrosion resistance is enhanced or at least not decreased[77].

Controversial reports are presented in case of γ_N. On one hand, in the corrosion test performed in NaCl-containing acidic environments with low pH, higher resistance to acid pitting corrosion is observed[78]. This is probably due to the release of reactive N in the solution where quadrivalent N combines with four hydrogen ions to form ammonium ions, thus reducing the acidity of the solution near the surface and increasing passive film stability. The same beneficial effect is observed with γ_C, even though no mechanism has yet been proposed[39].

On the other hand, corrosion resistance of γ_N in Cl^--free environment appears to be slightly reduced. Expanded austenite induces microstructural defects and high energy surfaces such as slip planes, twins and SFs, which tend to dissolve quickly in an acid environment. It can be assumed that γ_C would suffer less from this problem given the lower extent of internal stress-strain generated[79].

3.6 Applications

Austenitic stainless steels are often employed in industry mainly because of their high corrosion resistance, however their poor tribological properties often limit the range of application or impose high maintenance costs. For these reasons, in several applications it is certainly worthwhile for industry to invest in LTTT and form the expanded austenite case at the surface.

3.6.1 Nuclear industry

One of these examples is in the nuclear industry, where raw materials are not the main source of costs, but downtimes for safety maintenance are extremely costly and undesirable[80].

Control-rod cluster tubes are manufactured using austenitic stainless steel and their function is to hold neutron absorbing material to moderate nuclear reactions. The tubes tend to suffer from wear with their guide tubes due to repeated insertion-removal cycles and vibrations induced by hydraulic flow.

The whole control-rod cluster tubes can be plasma nitrided in large pit furnaces, with precise temperature control in order to assure a homogeneous heating throughout the tube and avoid charging and arcing defects. The treated tubes are not only superior to untreated SS, but also able to compete with those having anti-wear coatings such as chromium plating and chromium-carbide plasma spraying. Low-temperature nitriding treatment completely eliminated the necessary yearly replacement of the tubes[80].

3.6.2 Tube fittings and fasteners

Chemical, pharmaceutical, food and petrochemical industries employ austenitic stainless steel in the majority of their piping systems. Tubes fittings are necessary to connect pipes and withstand high pressure. One of the key elements is the “back ferrule”, which has the role of

gripping and sealing the tube[81]. To do so it has to be plastically deformed in a controlled manner to adhere on the pipe. Toughness, hardness, corrosion and galling resistance are desirable properties for such purpose.

Low-temperature carburizing treatment provides possibilities to meet these requirement. Kolsterising and Swagelok are viable commercial processes and standard practice for these applications nowadays.

3.6.3 Other applications

3.6.3.1 Ultraclean-sterile environments

Other applications include screws and nuts for high-purity gas fittings. The use of lubricants which might induce contaminations is avoided. At the same time galling is prevented. Avoiding lubricant residuals is of paramount importance for pharmaceutical and food industry. Dosing pumps for example are conventionally designed using rubber seals between cylinder lines and pistons to prevent adhesion wear. However they naturally degrade and might contaminate the final product[82]. Periodical replacement is required with consequent maintenance downtime. New pump-design can be achieved by applying a LTTT on both surfaces, reducing friction coefficient by several order of magnitude and considerably reducing operative costs of a plant.

3.6.3.2 Watches

Austenitic stainless steels are also growingly employed in jewellery and for consumer goods application. For example the majority of watch cases and wristbands are made of ASS. In this case the main purpose of a surface hardening treatment is aesthetic and to improve the scratch resistance. Low-temperature thermochemical treatments can also be used as a pre-treatment for a coating with low-friction coefficient such as DLC, increasing adhesion and load bearing capacity.

3.6.3.3 Biomedical

Prosthesis in biomedical applications are often made of austenitic stainless steel, with a growing trend of replacing Ni with Mn for biocompatibility reasons, or Co-Cr alloys as cheaper alternatives to titanium[83],[84]. Decreased wear rates through expanded austenite formation can significantly reduce risk of metal ions release in human bodies thus reducing toxic effects. At the same time, improved wear resistance decreases the necessity of implant replacement.

4 Experimental Techniques

4.1 Sample preparation

4.1.1 Sample preparation prior to surface treatment

Prior to nitriding, 304L and 904L plates were initially cut into 65 × 65 × 3 mm coupons. One side of the coupons was ground and polished until a 3-µm diamond paste to obtain a mirror-like surface. Another surface was left with the original surface finish, which was 2B (cold rolled, heat treated, pickled and skin passed) for 304L and 2E (cold rolled, heat treated and mechanically descaled) for 904L[85].

Prior to carburizing, for both materials 10 × 10 × 3 mm coupons were cut and one face was subsequently ground and polished until mirror-like using 1-µm diamond suspension.

Different sample sizes are used due to the different nature of the thermochemical treatments and the geometrical constrains of instruments used for subsequent characterizations.

For PN it is generally more convenient to have "large" parts (e.g. shafts), since they have to be electrically connected to the power supply and should not be in contact with each other in order to achieve a homogeneous treatment on the surface. However, several analytical instruments used in this work (e.g. SEM, XRD, XPS, GDOES) require a relative small sample size; therefore 10 × 10 × 3 mm specimens were cut from the larger nitrided coupons afterwards.

Gas carburizing techniques, instead, do not have size limitation and small parts (e.g. springs) can also easily be treated. Carburized samples could therefore be used without further preparation for most of the subsequent characterizations.

4.1.2 Preparation of cross-sections

Preparation of cross-sectioned samples was necessary to assess the expanded austenite thickness by means of either metallographic evaluation or backscattered electron imaging using scanning electron microscope. In all cases, cross-sections were mounted on conductive resin and polished with silica suspension.

4.1.2.1 Electroplating

Nickel plating was performed before cross-section preparation on carburized samples in order to retain sharp edge. Particularly, this is required for EBSD characterization, since the polishing step using extended silica suspension (OP-U) could have compromised the edge sharpness. Electroplating was performed by dipping the coupons in a 20-25% $NiSO_4$-10% $NiCl_2$ electrolytic solution for 60 min at a controlled temperature of 48°C and a constant voltage of 2.9 V between the substrate and the Ni plate used as anode.

4.1.2.2 Electrochemical etching

Phase contrast between expanded austenite and substrate on LTC cross-sections was not sufficient to effectively reveal the carburized layer by SEM. The high corrosion resistance of austenitic stainless steels, in particular for 904L, make electrochemical etching using stirred 20% oxalic acid solution necessary. A platinum electrode was used as a cathode and 8 V potential is applied for one minute.

4.2 Optical microscopic studies

Light optical microscopy (LOM) is a primary technique for studying the microstructure of steels. In this work, Leica and LEITZ DMRX microscopes were used in order to observe the effects of LTTT on the topography and microstructure of 304L and 904L (Fig. 11).

LOM was also used to estimate the carbon-stabilised expanded austenite layer thickness through examination of etched cross-section samples.

Optical profiler WYKO Rough Surface Tester Light Interferometer was used to measure the change in surface roughness caused by lattice expansion due to expanded austenite formation.

4.3 Scanning Electron Microscopy (SEM)

Scanning electron microscopy (SEM) has been of paramount importance in materials science thanks to the possibility to overcome the wavelength limit of visible light of LOM thus allowing significantly higher resolution. In addition, thanks to backscattered electron imaging it is possible to obtain information of composition contrast on different phases present in the material without etching procedure.

In SEM, electrons are generated by a source (tungsten, LaB_6 or field emission gun) and accelerated through apertures at potential of several keV. The electron beam (EB) is then collimated and focused through an electron column by means of several electromagnetic lenses and is scanned on the specimen. High vacuum is necessary to increase electron mean free path, allowing high magnification and high resolution[86].

The electron beam interacts with matter producing a number of signals that can be depicted by different detectors and provide valuable information. Secondary electrons are generated by ionization of the atoms composing the material. Having low kinetic energy, they can only escape from the depths in the order of ~ 100 nm (Fig. 12), providing valuable information on the topography. Backscattered electrons are a result of elastic scattering of the primary electron beam and being highly energetic, the information volume of backscattered electrons corresponds to a lateral resolution in the range of ~ 1 μm; the backscatter yield is dependent on the atomic number of the elements present in the material. Heavy elements backscatter electrons more strongly than light elements, therefore presence of different phases induce image contrast. This effect was used in this study to measure expanded austenite thickness in LTN materials.

X-rays are generated as a consequence of electrons decaying to fundamental state after ionization. These X-rays come from an interaction volume that provides the lateral resolution of 1 ~ 10 μm, characteristic for each element and dependent on primary electron beam energy. The X-ray signal can then be used for chemical composition analysis through energy-dispersive X-ray spectroscopy (EDX). A significant part of the characterizations in this study was performed using a FEG-SEM Leo Gemini 1550 for high resolution imaging in conjunction with Oxford Inca and Aztec (EDX) systems for chemical analysis and electron back-scattered diffraction (EBSD) using Oxford Nordlys.

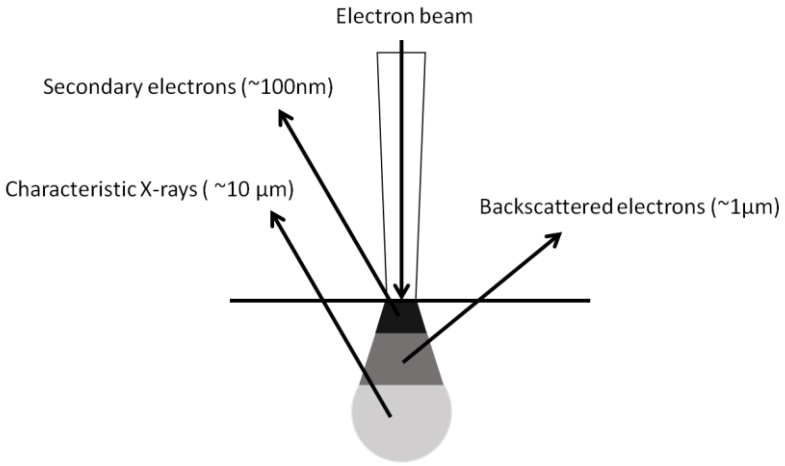

Figure 12 Schematic electron beam-sample interaction volume and signals generated in SEM.

4.3.1 Electron backscattered diffraction (EBSD)

Electron backscattered diffraction (EBSD) is a characterization technique that gives crystallographic and microstructural information with high spatial resolution. It is based on the diffraction (see section 4.4) of backscattered electrons and therefore it is a powerful tool for SEM systems. The EB interacts with a crystalline material and diffraction cones are generated, which is detected by a fluorescent screen and recorded with a camera. Analysis of cone arcs (Kikuchi lines) patterns allows for example to identify the crystal structure, orientation, presence of texturing in the material and study the grain boundaries[87].

Among the many applications of EBSD, in this work we focused on phase identification and strain analysis through average local misorientation maps[88] (Paper III). Misorientation depth profiles were averaged between five profiles in correspondence of nanoindented areas. Averaged misorientations below 0.2° are considered background.

4.4 X-ray diffraction (XRD)

X-ray diffraction is probably the most commonly used analytical technique for phase identification. The working principle is based on diffraction of X-rays (Fig. 13) as described by the Bragg´s law (eq. 12):

$$n\lambda = 2d \sin\theta \qquad (12)$$

Where n is the diffraction order, λ is the wavelength of the X-ray source, d is the diffraction interplanar distance and θ is the diffraction angle[89].

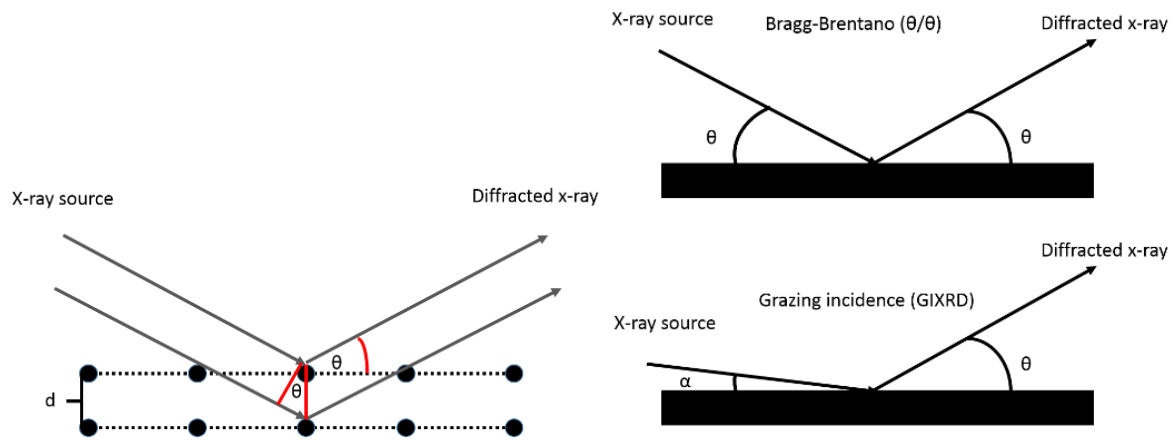

Figure 13 Left: schematic x-ray diffraction principle. Right: schematic θ/θ and grazing incidence XRD configurations.

Phase identification is performed by measuring the angles where constructive interference of X-rays is located and then converting into interplanar distance. Sets of diffracting planes are then matched with those from the standard database (Powder Diffraction Files from the International Centre for Diffraction Data).

From sets of interplanar distances it is then possible to calculate the lattice constants, which for cubic systems is *a* (eq. 13):

$$\frac{1}{d^2} = \frac{h^2+k^2+l^2}{a^2} \qquad (13)$$

Where *hkl* are the Miller indexes.

The instrument employed in this work is a Bruker AXS D8 Advance system equipped with a CrK_α radiation source (λ = 2.29 Å) and a Göbel mirror. It was used both in Bragg-Brentano *θ/θ* and grazing incidence (GIXRD) configuration. Analysis step size was chosen to be 0.05° with 5 s collection time and generator was set at 35 kV acceleration voltage and 40 mA current.

In *θ/θ* configuration both source and detector move along an arc with the same angular speed, while in GIXRD the incident beam is at a fixed angle α while the detector scans along the diffraction arc (see Fig. 14). The main difference of these two techniques is the depth of information, which is limited to ~ 1 µm for GIXRD depending on the incident angle and the material analysed. It is useful for determination of phase constituents in the near surface region at the expenses of lower counts especially at high diffraction angles. The *θ/θ* configuration has to be considered as a ”bulk” analysis techniques since it probes several µm in depth and the information depth varies significantly from low to high diffraction angles (90% absorption is ~ 5 µm at *2θ* = 60° and ~ 10 µm at *2θ* = 130° as calculated by AbsorbDX software for 904L chemical composition).

4.5 X-ray photoelectron spectroscopy (XPS)

X-ray photoelectron spectroscopy is a surface sensitive characterization technique for chemical analysis (also known as ESCA that stands for electron spectroscopy for chemical analysis), having a depth of information up to about 10 nm below the materials surface. When used in combination with an Ar ion gun it is possible to perform concentration depth

profiling. Among its advantages is the possibility of quantitative detection of almost every elements in the periodic table (excluding H and He), including light elements such as O, C or N in a metal matrix. It is also commonly used to identify the chemical state of the species present in the studied material.

The working principle of this technique is based on ionization through X-ray irradiation (Fig. 14). An X-ray source shines radiation on the sample surface producing ejected core electrons or valence electrons of the atoms composing the material. The kinetic energy and the intensity of the photoelectron are then recorded by a detector. The binding energy, specific for each element can be calculated using the following equation (eq. 14):

$$E_B = h\nu - E_K - \phi \qquad (14)$$

Where E_B is the binding energy, $h\nu$ photon energy, E_K kinetic energy and ϕ work function of the instrument[90].

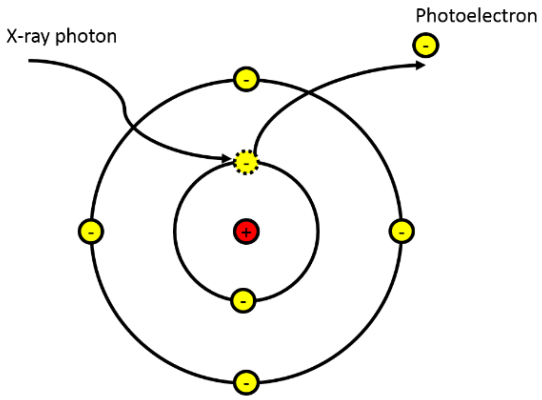

Figure 14 Schematic X-ray photoemission process.

Since the technique relies on analysis of electrons kinetic energy, an ultra-high vacuum is required (< 10^{-8} mbar). The standard experimental procedure includes survey spectra acquisition with broad binding energy window for general chemical composition analysis. High energy resolution spectra of specific core levels from elements of interest allow identification of chemical state.

It is important to remember that the Ar^+ etching necessary for depth profiling induces a progressive chemical and structural damage on the material. Preferential sputtering (usually of light species), increased roughness and even change of chemical state are common artefacts and need to be considered when performing depth profiles.

In this study, the analyses were done using a PHI5500 spectrometer, having a monochromatic AlKα X-ray source ($h\nu$ = 1,486.6 eV). Experimental conditions were 93.9 eV pass energy with step size 0.4 eV/step for survey spectra, while the pass energy was 23.5 eV for high resolution spectra with 0.1 eV/step. In both cases the take-off angle was 45°.

XPS was used to determine the chemical composition in the near-surface region. It was also applied in Paper I to determine different chemical shift present in N-supersaturated expanded austenite compared to CrN-like compounds. In this case, to remove surface contamination without altering the chemical nature of the species significantly, a low energy ion etching (1 keV) was used.

4.6 Glow-discharge optical emission spectroscopy (GDOES)

Glow-discharge optical emission spectroscopy (GDOES) is a destructive chemical analysis technique routinely used for time efficient concentration depth profiling of relatively thick layers or coatings (several tenths of µm). Another advantage of GDOES is the high sensitivity to both light and heavy elements.

A potential is applied between an electrode and the sample (cathode) in order to trigger a plasma discharge in an inert gas at low pressure, as shown in Fig. 15. Sputtering processes progressively remove atoms from the sample. Atoms ejected interact with the plasma and then emit characteristic X-photons which pass through a monochromator and finally are collected by photomultipliers. By analysing the electric signal generated, quantitative information of material composition is obtained.

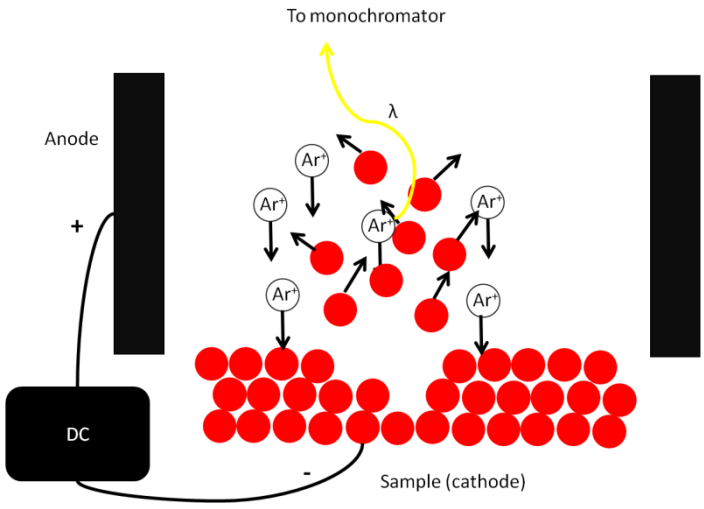

Figure 15 Schematic working principle of glow-discharge optical emission spectroscopy (GDOES).

The instrument used in this work is a Spectruma GDA750HP equipped with a DC source and a 2.5 mm diameter brass anode. The glow was obtained in argon (5.0 purity) with an average pressure of 500 Pa. The average erosion rate was 0.0875 µm/s, which was determined experimentally by measuring the crater depth using a stylus profilometry (KLA-Tencor Alpha step profilometer). Optimized depth resolution was confirmed by the flat crater, which had small roughness (R_a < 1 µm at depth of 35 µm).

Semi-quantitative depth profiles were obtained assuming a constant elemental emission yield and a linear relationship between concentration and emission intensity. Atomic concentration of C measured by XPS after contamination removal on carburized 904L from our Paper II was taken as the reference for the quantification.

4.7 Hardness measurements

Hardness is not an intrinsic material property but is dependent on a series of factors such as stiffness, ductility, strength, toughness and viscoelasticity. A large variety of hardness measurements techniques are available. For metals the most widespread are the so called “indentation techniques”.

In general, indentation techniques measure the resistance of a material to plastic deformation induced by an indenter having a specific geometry with a specific applied load (L) kept for a specified time. For Vickers hardness, a squared base pyramid indenter having angle of 136° is employed and the hardness is calculated by dividing the load with the area of indentation footprint as follows (eq. 15):

$$HV = \frac{L}{A} = \frac{2\sin\left(\frac{136^\circ}{2}\right)L}{d^2} \qquad (15)$$

Where d is the average diagonal of the indentation.

While hardness measurements are conventionally performed on the surface of the specimen, this is not highly recommended for LTTT ASS for several reasons. First of all, after low temperature carburizing/nitriding procedure, surface roughness increases up to the point that indentations have an irregular shape thus compromising the quality and repeatability of the measurement. Secondly, it is very likely that a certain contribution of the substrate will emerge since strain field extends in average about ten times the depth of the actual indentation. Moreover, this contribution will be dependent on the applied load and potentially on the holding time (creep).

To further reduce the strain-field volume and achieve higher spatial resolution in the measurement, nanoindentation is a convenient technique. In this case the applied load can be much lower (nN) and hardness can be calculated in real time from the load-displacement curve recorded by the instrument.

For the reasons mentioned above together with the relatively small thickness of hardened case (20 - 30 µm), both microhardness and nanoindentation hardness profiles were obtained on polished cross sections. The distance between indentations (> 3d) follows ASTM E384/ISO 6507-1 standards, in order to avoid interaction of deformation field. However, the distance from the edge of the sample could not always be assured due to the geometry limitation of the sample. The nanoindentation measurements were coupled with local misorientation maps, which represent strain levels in the material, helping to de-couple different contributions of hardening mechanisms.

The microhardness depth profiles (Paper II) were performed using a Shimadzu HMV-2000 (L = 10 gf, T = 10 s), with indentation size being evaluated with an optical microscope. The nanoindentation (Paper III) was performed with a CSIRO UMIS equipped with a Berkovich tip (L= 5 mN load, T = 10 s).

5 Summary of results and discussion

This thesis is the result of the work carried out in the last three years, which led to the three appended publications. The aim of this study was to characterize the microstructural characteristics of expanded austenite formed in two austenitic stainless steel alloys, 304L and 904L. The case hardening was performed by applying two industrial LTTT, namely PN and LTC. The aim was to study the influence of alloying elements and surface finishing on the material response to such treatments. In particular the concentration and distribution as well as the chemical bonding of interstitial species, morphology, thermal stability and hardening mechanisms of as-formed and decomposed expanded austenite were analysed and discussed through a multi-technique analysis approach.

Paper I presents the characterization results of low-temperature plasma nitrided austenitic stainless steels. Two PN conditions with varied N partial pressure and treatment time were applied. Paper II and Paper III are focused on carbon stabilized expanded austenite induced by Kolsterising K22 surface treatment on 304L and 904L.

5.1 Topography of treated surfaces

The surface morphology changes as a consequence of the treatments. The microstructure (austenite grain structure) is revealed without need of etching except for highly nitrided P304L-H due to extensive decomposition during the process. In addition, the surface roughness increases. There is a relationship between lattice expansion and increase in surface roughness (Paper II). Carbon expanded austenite induces almost double increase in roughness in 904L compared to 304L. The interstitial diffusion is anisotropic, leading to anisotropic stresses which in turn gives rise to asynchronous and non-uniform plastic deformation. Consequently, the grain structure is revealed and surface roughness is increased. It should be mentioned that there is a plasma etching effect for nitrided samples, which seems to be non-uniform over the surface. This results in contemporary presence of a dull central area and a reflective region.

In all examined materials (except for highly nitrided P304L-H), twins and slip bands are observed on the surface, indicating plastic deformation due to large internal stresses. The effect of nitrogen on lowering SF energy in austenitic stainless steel has been well known and carbon seems to have similar effects. Highly nitrided 904L also exhibited cracking due to high internal stresses resulting from incorporation of large amount of N atoms.

5.2 Layer thickness of expanded austenite

The thickness of case hardened layer reflects the diffusion depth of interstitial species and is of great importance for applications involving load bearing. Table 2 summarizes the layer thickness of expanded austenite for plasma nitrided (Paper I) and Kolsterised (Paper II) 304L and 904L. Measurements were performed on cross sections.

The S-phase thickness was less uniform within plasma nitrided samples (L condition), possibly due to charging effects during the process. For this reason the relative standard deviation of average case thickness is significantly higher for γ_N compared to γ_C.

Table 2 Summary of nitrided layer thickness for plasma nitrided (Paper I) and carburized layer thickness Kolsterised (Paper II) 304L and 904L.

Material and surface	Process type	Layer thickness (μm)	Surface at%*
P304L-L	LTN	4.4 ± 2.0	18-21
P304L-H	LTN	39.6 ± 3.9	18-20
N304L-L	LTN	8.0 ± 0.5	14-15
N304L-H	LTN	44.1 ± 4.1	n.d.
304L K22 P	LTC	24.3 ± 1.9	11
304L K22 NP	LTC	26.9 ± 1.4	13
P904L-L	LTN	4.3 ± 0.6	9-10
P904L-H	LTN	18.9 ± 2.0	18-20
N904L-L	LTN	5.8 ± 1.0	n.d.
N904L-H	LTN	25.9 ± 3.7	n.d.
904L K22 P	LTC	24.0 ± 1.0	18
904L K22 NP	LTC	25.2 ± 1	21

** Surface concentration of interstitial atoms was measured by XPS for nitrided samples and GDOES for carburized samples.*

There is a clear trend for both treatments that non-polished surfaces with original surface finishing (cold rolled for 304L and sandblasted for 904L), is beneficial for interstitial diffusion. The reason is probably the presence of surface defects caused by finishing operation which allows fast diffusion paths for interstitial atoms.

5.3 Phase constitution of surface engineered austenitic stainless steels

5.3.1 Low temperature nitriding

Plasma nitriding induced a complex compound layer on 304L surfaces. The CrN-like compounds, Fe_4N and Fe_3N were found on highly nitrided 304L (H condition), which suggests a complete decomposition of expanded austenite layer. For the less severely nitrided L-condition instead, the nitrided surface was more stable and with a thinner compound layer. The XRD pattern of P-surface suggests the presence of expanded austenite and $Fe_{16}N_2$ (α´´), a precursor of Fe_4N,[91] within the area with thicker expanded austenite layer. The CrN and no lattice expansion were identified in "Area 2". This behaviour can be explained by the fact that the supersaturation threshold is not being reached for the N-condition, owing to the fast interstitial diffusion. In P-surface, deformation induced martensite acted as a diffusion barrier.

High alloyed 904L on contrary shows dominant presence of expanded austenite. A very thin superficial CrN compound was detected only in L condition by GIXRD analysis. Our results confirm the theory that higher alloyed steel reduce the thickness of the compound layer[27].

By selectively removing the thin compound layers it was possible to evaluate the chemical bonding of Cr and N within the S-phase. The binding energies of Cr $2p_{3/2}$ and N 1s from expanded austenite were located at 574.5 eV and 397.3 eV respectively. Chemical shift of XPS peaks with respect to CrN were about - 0.3 eV compared to metallic Cr and + 0.3 eV for N peak compared to N in CrN (Fig. 16).

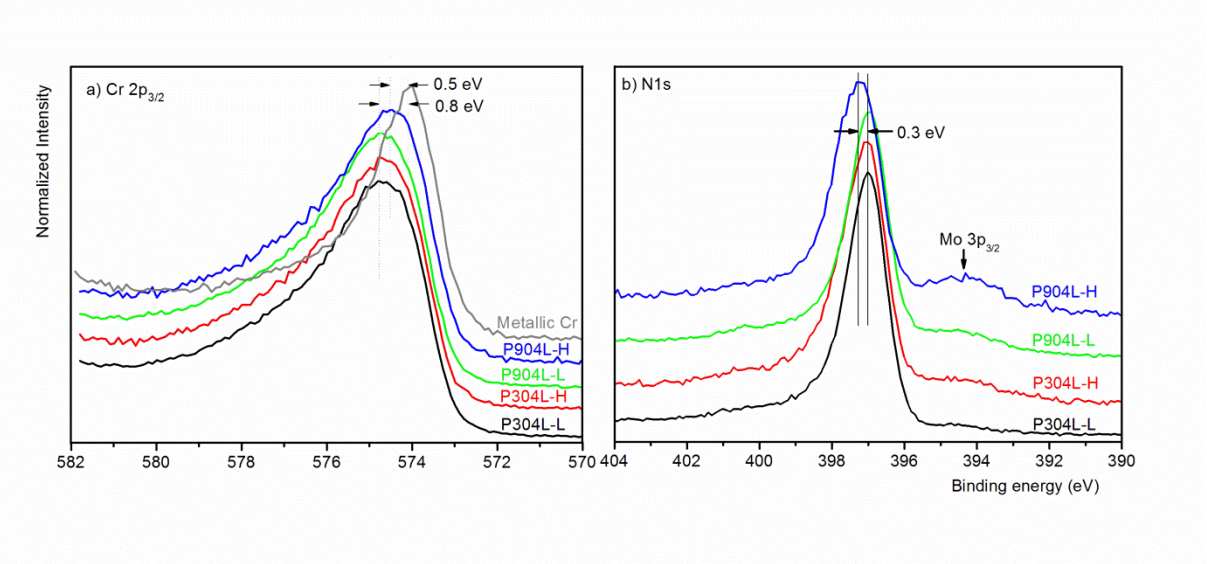

Figure 16 XPS a) $Cr2p_{3/2}$ and b) N 1s peaks from as-nitrided materials (Paper I)

These results differ from those reported by Riviere et al.[92] who claim that the binding energy of Cr and N in S-phase are within the range of those characteristic of CrN. These authors have used energetic 5 keV Xe^+ ion sputtering to remove surface contamination. Such high energetic ions might have caused chemical reactions at the surface (adventitious carbon combines with Cr forming carbides). The controlled polishing followed by 1 keV Ar^+ sputtering, in the present licentiate thesis study, is considerably more "gentle" and should have maintained the original chemical state of the species. In fact, our result shows an intermediate XPS peak position between metallic Cr and CrN for the $Cr2p_{3/2}$ peak, which confirms a different short range ordering compared to that of pure nitrides, as suggested by Oddershede et al. using EXAFS measurements[49].

5.3.2 Low temperature carburizing

The study performed on carburized 304L (Paper II) showed presence of χ-Hägg carbides in the near-surface region beside S-phase, while mainly S-phase was observed on 904L. The χ-Hägg carbide which is considered as "unusual" in austenitic stainless steels was previously reported by Cao et al. on 316L stainless steel treated by "Swagelok" process[69]. The authors associated its formation with the stabilizing role of Mn present in 316L. Manganese is present in both alloys of our study with equivalent amount. However such type of carbides is not identified within 904L. Hägg carbides are also known to be part of the catalytic reaction product when Fe reacts with CO + H_2 when forming hydrocarbides[93] in temperature ranges compatible with those of LTC treatments (> 200˚C). Therefore another hypothesis could be the presence of BCC-like phases (δ-ferrite or martensite) on the materials surface to induce their formation. According to Schaeffler-diagram, both 304L and 316L are located within the three phase region (A + F + M), while 904L is in the single austenite region.

5.4 Interstitial content

The interstitial content in the near surface region for nitrided steels was quantified by means of XPS analysis. The ratio of N/Cr in depth profile also allowed the estimate the thickness of the compound layer eventually present on the surfaces. The thickness of the compound layer

can be as large as 160 nm for 304L, while it is only a few tens of nm for 904L. Lower nitriding potential and shorter nitriding time in the L-condition caused generally lower intake of N in the ASS, which in turn lead to a higher tendency in forming surface nitrides given the lower diffusivity of interstitial at lower concentrations.

Carbon concentration in ASS treated with Kolsterising was estimated both directly and indirectly by XRD peak shift and GDOES depth profile calibrated with XPS values (Fig. 17). Narrow XRD peaks in 304L suggest a rather homogeneous carburizing within the probed depth, while 904L peaks show significant peak broadening and asymmetry. When treated in the same conditions, 904L shows a saturation threshold almost 8at% higher compared to 304L. Non-polished surfaces consistently dissolve higher amounts of interstitial due to higher pre-existing plastic deformation and consequently larger dislocation density, increasing solubility and favouring diffusivity[94]. Moreover, considering the C concentration profile in 904L the NP condition shows a steeper gradient and a higher maximum supersaturation compared to P condition. This could suggest that the maximum limit in the concentration-dependent diffusion was trespassed, hence diffusion was hindered due to lower interstitial-jumping probability.

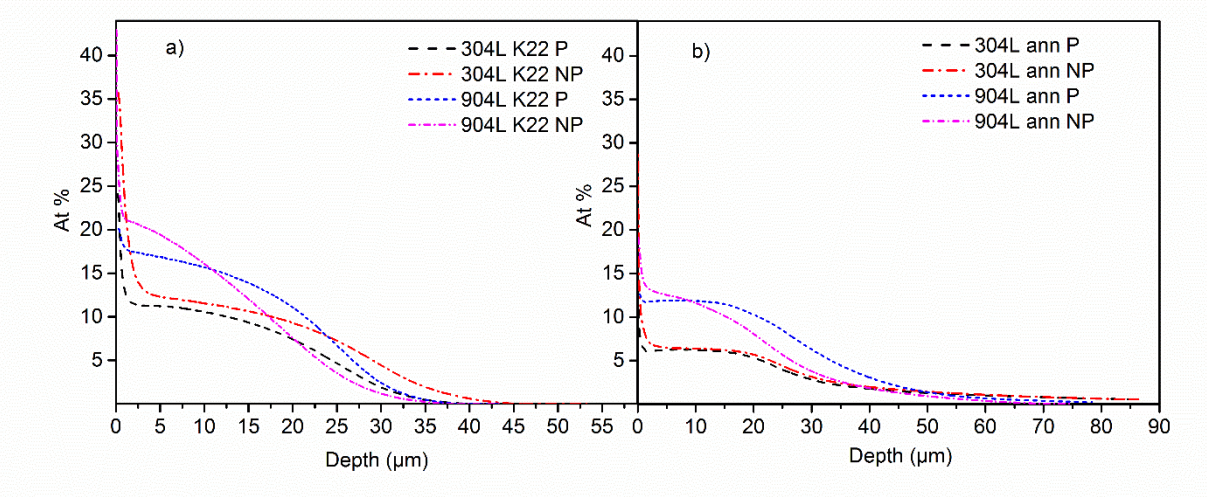

Figure 17 GDOES carbon concentration profiles of (a) low-temperature carburized 304L and 904L, (b) after vacuum annealing at 600˚C for 150 h.

Interestingly, the layer thickness of expanded austenite measured by optical microscopy does not correspond to the one measured by GDOES depth profile. Apparently there is an effective threshold of interstitials necessary to induce sufficient resistance to etching compared to pristine ASS.

5.5 Thermal stability of expanded austenite

The thermal stability of expanded austenite was evaluated considering two factors: formation of compounds (precipitates) during the thermochemical treatments and phase evolution during extended vacuum annealing (only in carburized materials).

From all experiments performed it can be generalised that expanded austenite is more stable in 904L than in 304L. The compound layers were significantly thinner (or not present at all) in the former compared to the latter in all cases. The lower alloyed 304L could not form or maintain nitrogen stabilised expanded austenite structure at 400˚C for 99 h (Paper I).

When annealing at conditions where complete expanded austenite decomposition occurs, three separated phenomena compete during the process: a) decarburization in all materials with maximum C content at the surface, b) inward diffusion of interstitials confirmed by GDOES and c) carbides formation. Complete expanded austenite decomposition is accompanied by thorough relaxation of lattice strain, suggesting removal of C/N from interstitial solid solution.

We confirmed the presence of two different decomposition routes for the two studied materials. Lower alloyed 304L follows either a eutectoid or a mixed-type decomposition route (eq. 10 and 11), depending on the surface finishing. Mechanical polishing causes deformation induced martensitic transformation, which possibly provides nucleation sites for ferrite after annealing. The final microstructure is a thick layer of ferrite with finely dispersed chromium-rich carbides and a small amount of residual austenite phase (Fig. 18). It should be noticed that the grain size of newly formed ferrite is significantly smaller than austenite. Carbides are mainly located at grain boundaries of ferrite, but they also can be found within the grains. The non-polished side instead shows a mixed decomposition route. However, ferrite is formed mainly at the top surface below which discontinuous decomposition is dominant with some carbides and ferrite at the grain boundaries of unexpanded austenite.

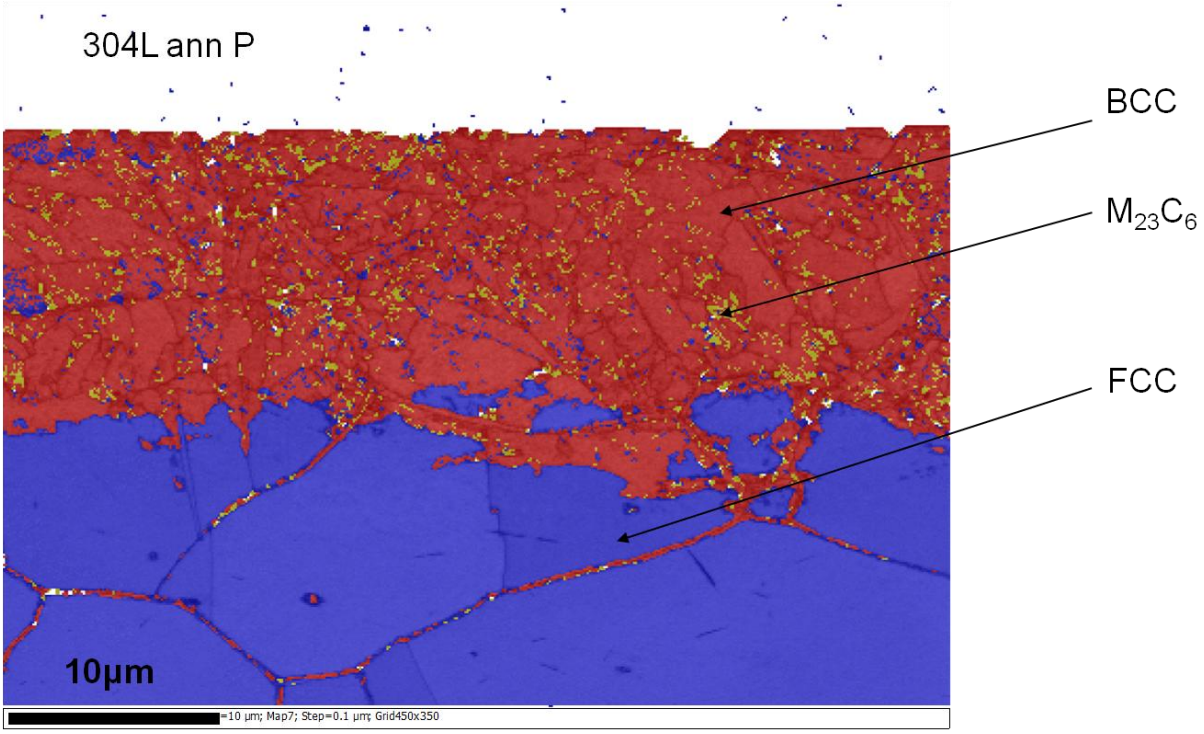

Figure 18 EBSD phase composition map of cross-sectioned annealed 304L, polished surface (unpublished result).

High alloyed 904L always followed a discontinuous decomposition path (eq. 11). Preferential precipitation sites for carbides formation were grain boundaries, slip bands and twin boundaries. The decomposition mechanism for 904L is fairly in line with hypothesis available in literature for 316 type steel[73]. Given the high thermodynamic stability of austenitic phase, discontinuous decomposition is the only possibility available.

Both alloys present formation of $M_{23}C_6$ type carbides after annealing, even though interstitial content after LTC was still so high that would suggest the presence of higher order carbides in 904L[40].

5.6 Hardening mechanisms

For as-carburized surfaces, the major contribution is solid solution hardening by interstitial and "work hardening" (Paper II). Work hardening in this context means increase of dislocation density due to deformation resulted from internal stresses. Presence of micro-twins could not be detected with our techniques but cannot be excluded. Non-polished surfaces exhibit a deeper strained region, probably caused by a combination of pre-existing plastic deformation from the original surface finishing (skin pass or sandblasting) and consequently enhanced expanded austenite supersaturation, inducing sufficient misorientation within the grains to be detected by our EBSD measurements (Paper III).

Partial hardening effect is maintained in most cases after annealing at 600^{o}C, except for discontinuously decomposed 304L. The hardening mechanism in this case is related to the surface finishing prior to carburizing and steel composition. Solid solution hardening from interstitials is now negligible. Grain size strengthening due to the formation of small ferrite grains and the related strain hardening, possibly due to the strain field induced by interphase lattice mismatch, are responsible mainly for the maintained hardness enhancement for polished 304L. We believe that precipitation in 304L ann N sample, being restricted to the grain boundaries, does not contribute to hardening. In the case of 904L, instead, precipitates at original twin boundaries and slip bands provide hardening effect. The hardening seems to extend beyond the original expanded layer towards the bulk, probably as a consequence of further interstitial diffusion during annealing.

6 Conclusions

This work is focused on studying the microstructure, chemical bonding and thermal stability as well as hardening mechanisms involved in expanded austenite formed 304L and 904L austenitic stainless steels treated by PN and LTC. Chemical composition, phase constitution and surface finishing of the materials tested have proven to be important to the interstitial diffusivity, thermal stability and hardening effects in expanded austenite.

It has been found that these LTTT lead to C/N supersaturation up to ~ 20at% in both stainless steels. A well-defined layer of expanded austenite can be formed. Alloy 904L has shown higher stability in both N and C stabilised expanded austenite. Compared to 304L, the thickness of compound layer was consistently smaller and interstitial saturation threshold was generally higher. Meanwhile, formation of detectable Cr-rich precipitates was less likely. Significantly higher amount of Ni acting as austenite stabilizer in 904L reduced the risk of the formation of BCC-like phases, therefore increasing stability of expanded austenite. The typical low interstitial solubility due to Ni seems to be compensated by presence of alloying elements with larger atomic radii such as Mo and Cu, having role of increasing the average lattice parameter thus facilitating diffusion.

Alloy 304L was more susceptible to deformation induced martensite. This phase together with pre-existing δ-ferrite can be an obstacle for expanded austenite formation and consequently favour the formation of Cr-compounds, detrimental for corrosion resistance.

It has also been found by XPS analyses that the bonding feature of Cr-N in expanded austenite differs from that of conventional CrN. However, short range ordering does exist.

Original surface finishing has considerable influence on the kinetics of S-phase formation and its stability as well as interstitial solubility. Presence of deformation induced martensite makes the formation of expanded austenite less favourable, reducing the expanded austenite thickness. Pre-existing plastic deformation caused by sandblasting or cold-rolling provides fast diffusion paths for interstitial diffusion. Moreover, presence of high-dislocation density areas seems to enhance interstitial solubility.

Decomposition mechanisms of carbon expanded austenite in both steels as well as its dependency on surface finishing were also shown for the first time. Upon annealing at elevated temperatures, decarburization, carbide formation and C diffusion into the bulk take place. The expanded austenite in 304L decomposes following either eutectoid or a mixed route, depending on the surface finishing. We hypothesise that deformation induced martensite, formed during mechanical polishing, may acts as nucleating site for ferrite nucleation. Superaustenitic 904L, instead, decomposes through discontinuous route.

On average, a four-fold increase in hardness is observed at the surface after LTC. Solid solution hardening and “work hardening” caused by internal stresses are the main responsible mechanisms, the latter of which is less important for 304L. Upon annealing, softening to different degree is observed. Remaining hardening effect in case of eutectoid decomposition in 304L can be explained by grain size strengthening and interphase strain hardening. In case of discontinuous decomposition in 904L, strain hardening caused by carbide precipitate along twin boundaries or slip bands is the main contributing mechanism.

7 Future studies

In our future studies we plan to expand the work regarding the effect of alloying elements and multiple phases on the structure, properties and thermal stability of expanded austenite. In particular, we intend to systematically assess the competing effects of Ni and Mo/Cu in terms of solubility and diffusivity of interstitials. Moreover, the role of sulphur and its interactions with key alloying elements during formation of expanded austenite will also be subject of our future research.

Another focus is the short range ordering of metallic element Cr with interstitial carbon by means of combined spectroscopic approach, e.g. XPS, Auger, UPS, Raman.

The applications of low-temperature hardened austenitic stainless steels in the field of energy conversion devices will also be of great interest. Specifically, we will explore the potential of expanded austenite as bipolar plats for polymer electrolyte membrane fuel cells by paying close attention to electrochemical corrosion resistance and electrical conductivity of the surface.

8 Acknowledgements

First and foremost I would like to thank my supervisors, Asso. Prof. Yu Cao and Prof. Lars Nyborg, for their constant support and guidance in the last three years. Their knowledge and commitment were fundamental for the development of this work and for my growth as a scientist.

Heinz Kaiser and Bodycote Värmebehandling (Sweden) are highly acknowledged for providing the surface treatments on which the current thesis is based upon. In particular, special thanks go to Fredrik Carlsson who introduced us to Kolsterising.

National School of Materials Science, Area of Advance Materials Science and National Swedish Energy Administration are acknowledged for financial support of this PhD project. Jernkontoret and Chalmersska Forskningsfonden are also to be thanked for providing financial support.

I would like to thank our research engineers: Urban Jelvestam, Dr. Eric Tam, Dr. Yiming Yao and Roger Sagdahl for all the practical support and standing my rather frequent "Just a small question…" and "I think we have a problem with…". I believe you deserve a statue for your patience and kindness!

Many thanks to all the co-authors of the papers included in this thesis, starting from Dr. Mats Norell for the thorough discussions, Dr. Simone Vezzù and Dr. Alfonso Perez Garcia for the enthusiasm and effort in long-distance cooperation, Dr. Lina Rogström for the interest in my research.

I would like to express my sincere gratitude to all the members and colleagues working in Department of Materials and Manufacturing Technology.

In particular I would like to thank the colleagues and friends who already left or are about to finish their career as PhD students: Lic. Eng. Christos Oikonomou (who I will soon miss!), Lic. Eng. Amir Malakizadi, Dr. Seshendra Karamchedu, Dr. Erik Stenvall, Dr. Kumar Babu Surreddi, Dr. Stefan(O) Cedergren, Dr. Ruth Ariño Marine for being so friendly from the first day of my arrival in this department. Friendship that extended also outside these four walls, I wish you all the best!

Continuing with colleagues and friends, I would like to thank Dinesh Mallipeddi, Kristina Karlsson, Casey Jessop, Antonio Mulone, Johanna Ekberg, Philipp Hoier, Sakari Tolvanen, Maheswaran Vattur Sundaram, Dimitris Nikas and Elanghovan Natesan. Many more discussions, fika breaks, innebandy and teaching duties (!) have to come.

I would like to thank my Family and the friends of a lifetime, who never lack in making me feel as if I was always there with them.

Dulcis in fundo, a great thank you to my girlfriend Giedre Asmonaite: without you I would not even be here (in Sweden) in the first place! Not to mention the loving understanding and ENORMOUS patience you have with me.

The final dedication is to my parents, you are always in my mind and in my heart.

9 References

[1] W. Krivsky, “The linde argon-oxygen process for stainless steel; A case study of major innovation in a basic industry,” *Metall. Mater. Trans. B*, vol. 4, no. 6, pp. 1439–1447, 1973.

[2] Outokumpu, “Handbook of Stainless Steel,” 2013.

[3] Issf, “Stainless steel in figures 2013,” pp. 5–7, 2013.

[4] M. F. McGuire, *Stainless Steels for Design Engineers*. ASM International, 2008.

[5] B. D. Miller, “Precipitation Behavior of M 23 C 6 Carbides in Type 304 Stainless Steel Containing Delta Ferrite,” *Microsc. Microanal.*, vol. 1, no. Suppl 2, pp. 1352–1353, 2012.

[6] M. A. Martorano, C. F. Tavares, and A. F. Padilha, “Predicting Delta Ferrite Content in Stainless Steel Castings,” *Adv. Mater. Forum VI*, vol. 52, pp. 733–738, 2013.

[7] A. F. Padilha and P. R. Rios, “Decomposition of Austenite in Austenitic Stainless Steels,” *ISIJ Int.*, vol. 42, no. 4, pp. 325–327, 2002.

[8] R. P. Pascale Sotto Vangeli, Bo Ivarsson, “Comparative Behaviour of Speciality Austenitic Stainless Steels in High Temperature Environments,” *Acom*, no. 3, 2012.

[9] S. Jani, M. Marek, R. F. Hochman, and E. I. Meletis, “A Mechanistic Study of Transgranular Stress Corrosion Cracking of Type 304 Stainless Steel,” *Metall. Trans.*, vol. 22A, no. June, 1991.

[10] R. W. Swindeman, “Fatigue of Austenitic Stainless Steels in the Low and Intermediate Cycle Range,” 1966.

[11] A. G. Hartline, “The effect of nitrogen additions upon the pitting resistance of 18 pct Cr, 18 pct Mn Stainless Steel,” *Metall. Trans.*, vol. 5, pp. 2271–2276, 1974.

[12] Outokumpu, “Outokumpu Surface Finishes.”

[13] Outokumpu, “Standard Cr-Ni Stainless Steels,” 2006.

[14] G. F. Vander Voort, *ASM Handbook: Metallography and Microstructures*. 2004.

[15] S. Ghosh and V. Kain, “Microstructural changes in AISI 304L stainless steel due to surface machining: Effect on its susceptibility to chloride stress corrosion cracking,” *J. Nucl. Mater.*, vol. 403, no. 1–3, pp. 62–67, 2010.

[16] P. E. Manning, D. J. Duquette, and W. F. Savage, “Technical Note: The Effect of Retained Ferrite on Localized Corrosion in Duplex 304L Stainless Steel,” *Weld. Res. Suppl.*, no. September, pp. 260–262, 1980.

[17] M. Zandrahimi, M. R. Bateni, A. Poladi, and J. A. Szpunar, “The formation of martensite during wear of AISI 304 stainless steel,” *Wear*, vol. 263, no. 1–6 SPEC. ISS., pp. 674–678, 2007.

[18] A. K. De, D. C. Murdock, M. C. Mataya, J. G. Speer, and D. K. Matlock, “Quantitative measurement of deformation-induced martensite in 304 stainless steel by X-ray diffraction,” *Scr. Mater.*, vol. 50, no. 12, pp. 1445–1449, 2004.

[19] Outokumpu, “High Performance Austenitic Stainless Steel,” pp. 1–12, 2015.

[20] Outokumpu, “Ultra 904L,” pp. 1–7, 2015.

[21] B. N. Mordyuk, G. I. Prokopenko, M. A. Vasylyev, and M. O. Iefimov, “Effect of structure evolution induced by ultrasonic peening on the corrosion behavior of AISI-321 stainless steel,” *Mater. Sci. Eng. A*, vol. 458, no. 1–2, pp. 253–261, 2007.

[22] T. Wang, J. Yu, and B. Dong, “Surface nanocrystallization induced by shot peening and its effect on corrosion resistance of 1Cr18Ni9Ti stainless steel,” *Surf. Coatings Technol.*, vol. 200, no. 16–17, pp. 4777–4781, 2006.

[23] H. F. G. de Abreu, S. S. de Carvalho, P. de Lima Neto, R. P. dos Santos, V. N. Freire, P. M. de O. Silva, and S. S. M. Tavares, “Deformation induced martensite in an AISI 301LN stainless steel: characterization and influence on pitting corrosion resistance,” *Mater. Res.*, vol. 10, no. 4, pp. 359–366, 2007.

[24] X. . Wang and D. Li, “Mechanical and electrochemical behavior of nanocrystalline surface of 304 stainless steel,” *Electrochim. Acta*, vol. 47, no. 24, pp. 3939–3947, 2002.

[25] A. S. Lima, A. M. Nascimento, H. F. G. Abreu, and P. De Lima-Neto, “Sensitization evaluation of the austenitic stainless steel AISI 304L, 316L, 321 and 347,” *J. Mater. Sci.*, vol. 40, no. 1, pp. 139–144, 2005.

[26] T. M. Devine, “The mechanism of sensitization of austenitic stainless steel,” *Corros.Sci*, vol. 30, no. 2–3, pp. 135–151, 1990.

[27] D. Pye, “Steel Heat Treatment Metallurgy and Technologies,” in *Steel Heat Treatment Metallurgy and Technologies*, Boca Raton (FL): CRC Press, 2006.

[28] P. Weymer, “Principles of Gas Nitriding,” *Heat Treat. Prog.*, no. July/August, pp. 12–13, 2009.

[29] M. A. J. Somers and T. L. Christiansen, *Gaseous processes for low temperature surface hardening of stainless steel*. Woodhead Publishing Limited, 2015.

[30] T. Christiansen and M. A. J. Somers, “Characterisation of low temperature surface hardened stainless steel,” *Struers J. Mater.*, no. 9, pp. 1–17, 2006.

[31] E. J. Mittemeijer, “Fundamentals of Nitriding and Nitrocarburizing,” in *ASM Handbook, Volume 4, Heat treating Fundamentals and Processes*, ASM International.

[32] J. Elwart and R. Hunger, “Plasma (Ion) Nitriding and Nitrocarburizing of Steels,” in *ASM Handbook, Volume 4A, Steel Heat treating Fundamentals and Processes*, vol. 4, 2013, pp. 690–703.

[33] P. C. Collins, S.R., Williams, F. Marx, S.V. , Heuer, A.H., Ernst, and H. Kahn, “Low-Temperature Carburization of Austenitic Stainless Steels,” *ASM Handbook, Vol. 4D*, vol. 4, pp. 451–460, 2014.

[34] P. C. Williams, S. R. Collins, and S. V Marx, “Low Temperature Carburization Under Soft Vacuum,” US 2011/0030849 Al, 2011.

[35] T. L. Christiansen and M. A. J. Somers, “Low-Temperature Surface Hardening of Stainless Steel,” *Adv. Mater. Process.*, vol. 171, no. 11, pp. 52–53, 2013.

[36] Bodycote, “Specialty Stainless Steel Processes (S3P).” [Online]. Available:

http://www.bodycote.com/en/services/heat-treatment/specialty-stainless-steel-processes.aspx.

[37] Z. L. Zhang and T. Bell, "Structure and Corrosion Resistance of Plasma Nitrided Stainless Steel," *Surf. Eng.*, vol. 1, no. 2, pp. 131–136, 1985.

[38] K. F. Kazuo Ichii Takao Takase, "Structure of the Ion-Nitrided Layer of 18-8 Stainless Steel," *Technol. Reports Kansai Univ.*, vol. 27, pp. 135–144, 1986.

[39] H. Dong, "S-phase surface engineering of Fe-Cr, Co-Cr and Ni-Cr alloys," *Int. Mater. Rev.*, vol. 55, no. 2, pp. 65–98, 2010.

[40] T. Christiansen and M. A. J. Somers, "Low temperature surface hardening of stainless steel," in *Thermochemical Surface Engineering of Steels*, Woodhead Publishing Limited, 2015, pp. 557–579.

[41] M. P. Fewell, D. R. G. Mitchell, J. M. Priest, K. T. Short, and G. A. Collins, "The nature of expanded austenite," *Surf. Coatings Technol.*, vol. 131, no. 1–3, pp. 300–306, 2000.

[42] A. Martinavičius, G. Abrasonis, and W. Möller, "Influence of crystal orientation and ion bombardment on the nitrogen diffusivity in single-crystalline austenitic stainless steel," *J. Appl. Phys.*, vol. 110, no. 7, p. 074907, 2011.

[43] G. Abrasonis, J. P. Rivière, C. Templier, A. Declemy, S. Muzard, and L. Pranevicius, "A comparative study of ion beam nitriding of single-crystalline and polycrystalline 316L austenitic stainless steel," *Surf. Coatings Technol.*, vol. 196, no. 2005, pp. 262–266, 2005.

[44] C. Templier, J. C. Stinville, P. O. Renault, G. Abrasonis, P. Villechaise, J. P. Rivière, and M. Drouet, "Nitrogen interstitial induced texture depth gradient in stainless steel," *Scr. Mater.*, vol. 63, no. 5, pp. 496–499, 2010.

[45] M. P. Fewell and J. M. Priest, "High-order diffractometry of expanded austenite using synchrotron radiation," *Surf. Coatings Technol.*, vol. 202, no. 9, pp. 1802–1815, 2008.

[46] T. Christiansen and M. A. J. Somers, "On the crystallographic structure of S-phase," *Scr. Mater.*, vol. 50, no. 1, pp. 35–37, 2004.

[47] K. Farrell, E. D. Specht, J. Pang, L. R. Walker, A. Rar, and J. R. Mayotte, "Characterization of a carburized surface layer on an austenitic stainless steel," *J. Nucl. Mater.*, vol. 343, no. 1–3, pp. 123–133, 2005.

[48] G. M. Michal, F. Ernst, and A. H. Heuer, "Carbon paraequilibrium in austenitic stainless steel," *Metall. Mater. Trans. A*, vol. 37, no. June, pp. 1819–1824, 2006.

[49] J. Oddershede, T. L. Christiansen, K. Ståhl, and M. A. J. Somers, "Extended X-ray absorption fine structure investigation of nitrogen stabilized expanded austenite," *Scr. Mater.*, vol. 62, no. 5, pp. 290–293, 2010.

[50] J. Oddershede, T. L. Christiansen, K. Ståhl, and M. A. J. Somers, "Extended X-Ray absorption fine structure investigation of carbon stabilized expanded austenite and carbides in stainless steel AISI 316," *Steel Res. Int.*, vol. 82, no. 10, pp. 1248–1254, 2011.

[51] T. Christiansen and M. a. J. Somers, "Controlled dissolution of colossal quantities of nitrogen in stainless steel," *Metall. Mater. Trans. A*, vol. 37, no. 3, pp. 675–682, 2006.

[52] T. S. Hummelshøj, T. L. Christiansen, and M. A. J. Somers, "Lattice expansion of carbon-stabilized expanded austenite," *Scr. Mater.*, vol. 63, pp. 761–763, 2010.

[53] T. L. Christiansen and M. A. J. Somers, "Stress and Composition of Carbon Stabilized Expanded Austenite on Stainless Steel," *Metall. Mater. Trans. a-Physical Metall. Mater. Sci.*, vol. 40A, no. 8, pp. 1791–1798, 2009.

[54] S. Jegou, T. L. Christiansen, M. Klaus, C. Genzel, and M. A. J. Somers, "Determination of composition, residual stress and stacking fault depth profiles in expanded austenite with energy-dispersive diffraction," *Thin Solid Films*, vol. 530, pp. 71–76, 2013.

[55] J. Liu, P. Han, M. Dong, G. Fan, G. Qiao, and J. Yang, "Influence of Ni and N on generalized stacking-fault energies in FeCrNi alloy: A first principle study," *Phys. B Condens. Matter*, vol. 407, no. 5, pp. 891–895, 2012.

[56] D. L. Williamson, O. Ozturk, R. Wei, and P. J. Wilbur, "Metastable phase formation and enhanced diffusion in f.c.c. alloys under high dose, high flux nitrogen implantation at high and low ion energies," *Surf. Coatings Technol.*, vol. 65, no. 1–3, pp. 15–23, 1994.

[57] S. Parascandola, W. Möller, and D. L. Williamson, "The nitrogen transport in austenitic stainless steel at moderate temperatures," *Appl. Phys. Lett.*, vol. 76, no. 16, p. 2194, 2000.

[58] C. Blawert, B. L. Mordike, G. A. Collins, K. T. Short, Y. Jiraskova, O. Schneeweiss, and V. Perina, "Characterisation of duplex layer structures produced by simultaneous implantation of nitrogen and carbon into austenitic stainless steel X5CrNi189," *Surf. Coatings Technol.*, vol. 128–129, pp. 219–225, 2000.

[59] W. Möller, S. Parascandola, T. Telbizova, R. Günzel, and E. Richter, "Surface processes and diffusion mechanisms of ion nitriding of stainless steel and aluminum," *Surf. Coatings Technol.*, vol. 136, no. 1–3, pp. 73–79, 2001.

[60] T. L. Christiansen and M. a J. Somers, "Determination of the concentration dependent diffusion coefficient of nitrogen in expanded austenite," *Int. J. Mater. Res.*, vol. 99, no. 9, pp. 999–1005, 2008.

[61] T. Moskalioviene and A. Galdikas, "Stress induced and concentration dependent diffusion of nitrogen in plasma nitrided austenitic stainless steel," *Vacuum*, vol. 86, no. 10, pp. 1552–1557, 2012.

[62] G. Ubertalli, G. M. M. Mortarino, F. Rosalbino, and D. Firrao, "Indurimento superficiale di acciai inossidabili austenitici mediante tin-pvd e kolsterizzazione e loro caratterizzazione," *Metall. Ital.*, vol. 100, no. 4, pp. 15–20, 2008.

[63] M. Tsujikawa, S. Noguchi, N. Yamauchi, N. Ueda, and T. Sone, "Effect of molybdenum on hardness of low-temperature plasma carburized austenitic stainless steel," *Surf. Coatings Technol.*, vol. 201, no. 9–11 SPEC. ISS., pp. 5102–5107, 2007.

[64] W. Li, X. Li, and H. Dong, "Effect of tensile stress on the formation of S-phase during low-temperature plasma carburizing of 316L foil," *Acta Mater.*, vol. 59, no. 14, pp. 5765–5774, 2011.

[65] J. Baranowska, K. Szczeciński, and M. Wysiecki, "Increasing of gas nitriding kinetics via surface pre-treatment," *Surf. Coatings Technol.*, vol. 151–152, pp. 534–539, 2002.

[66] A. N. Allenstein, C. M. Lepienski, A. J. A. Buschinelli, and S. F. Brunatto, "Plasma nitriding using high H2 content gas mixtures for a cavitation erosion resistant steel," *Appl. Surf. Sci.*, vol. 277, pp. 15–24, 2013.

[67] C. Tromas, J. C. Stinville, C. Templier, and P. Villechaise, "Hardness and elastic modulus gradients in plasma-nitrided 316L polycrystalline stainless steel investigated by nanoindentation tomography," *Acta Mater.*, vol. 60, no. 5, pp. 1965–1973, 2012.

[68] B. Sartowska, J. Piekoszewski, L. Waliś, J. Stanisławski, L. Nowicki, R. Ratajczak, M. Kopcewicz, and J. Senatorski, "Thermal stability of the phases formed in the near surface layers of unalloyed steels by nitrogen pulsed plasma treatment," *Vacuum*, vol. 81, no. 10, pp. 1188–1190, 2007.

[69] Y. Cao, F. Ernst, and G. M. Michal, "Colossal carbon supersaturation in austenitic stainless steels carburized at low temperature," *Acta Mater.*, vol. 51, no. 14, pp. 4171–4181, 2003.

[70] X. Y. Li, S. Thaiwatthana, H. Dong, and T. Bell, "Thermal Stability of Carbon S Phase in 316 Stainless Steel," *Surf. Eng.*, vol. 18, no. 6, pp. 448–452, 2002.

[71] L. Wang, Y. Li, and Y. Z. Wang, "Thermal Stability of Nitrogen Expanded Austenite Formed by Plasma Nitriding on AISI304 Austenitic Stainless Steels," *Key Eng. Mater.*, vol. 373–374, pp. 308–311, 2008.

[72] L. Nosei, M. Avalos, B. J. Gómez, L. Nachez, and J. Feugeas, "Stability under temperature of expanded austenite developed on stainless steel AISI 316L by ion nitriding," *Thin Solid Films*, vol. 468, no. 1–2, pp. 134–141, 2004.

[73] T. Christiansen and M. A J. Somers, "Decomposition kinetics of expanded austenite with high nitrogen contents," *Int. J. Mater. Res.*, vol. 97, no. 1, pp. 79–88, 2006.

[74] M. K. Lei and X. M. Zhu, "Plasma-based low-energy ion implantation of austenitic stainless steel for improvement in wear and corrosion resistance," *Surf. Coatings Technol.*, vol. 193, pp. 22–28, 2005.

[75] Y. Sun and T. Bell, "Dry sliding wear resistance of low temperature plasma carburised austenitic stainless steel," *Wear*, vol. 253, no. 5–6, pp. 689–693, 2002.

[76] Y. Sun and T. Bell, "Effect of layer thickness on the rolling-sliding wear behavior of low- temperature plasma-carburized austenitic stainless steel," *Tribol. Lett.*, vol. 13, no. 1, pp. 29–34, 2002.

[77] Y. Zhao, B. Yu, L. Dong, H. Du, and J. Xiao, "Low-pressure arc plasma-assisted nitriding of AISI 304 stainless steel," *Surf. Coatings Technol.*, vol. 210, pp. 90–96, 2012.

[78] E. Menthe, K.-T. Rie, J. W. Schultze, and S. Simson, "Structure and properties of plasma-nitrided stainless steel," *Surf. Coatings Technol.*, vol. 74–75, pp. 412–416, 1995.

[79] L. Ceschini, C. Chiavari, E. Lanzoni, and C. Martini, "Low-temperature carburised AISI 316L austenitic stainless steel: Wear and corrosion behaviour," *Mater. Des.*, vol. 38, pp. 154–160, 2012.

[80] J. P. Lebrun, "Applications of low-temperature surface hardening of stainless steels," in *Thermochemical Surface Engineering of Steels*, Woodhead Publishing Limited, 2015,

pp. 633–647.

[81] S. Collins and P. Williams, “Low-Temperature Colossal Supersaturation,” *Adv. Mater. Process.*, no. SEPTEMBER, pp. 32–33, 2006.

[82] M. J. Bos, “Case Hardening of Austenitic Stainless Steel Pump Components,” *World Pumps*, no. March, pp. 30–34, 1998.

[83] J. Buhagiar, L. Qian, and H. Dong, “Surface property enhancement of Ni-free medical grade austenitic stainless steel by low-temperature plasma carburising,” *Surf. Coatings Technol.*, vol. 205, no. 2, pp. 388–395, 2010.

[84] J. Buhagiar, X. Li, and H. Dong, “Formation and microstructural characterisation of S-phase layers in Ni-free austenitic stainless steels by low-temperature plasma surface alloying,” *Surf. Coatings Technol.*, vol. 204, no. 3, pp. 330–335, 2009.

[85] *EUROPEAN STANDARD BS EN 10088 2:2005. Stainless steels - Part 2 : Technical delivery conditions for sheet / plate and strip of corrosion resisting steels for general purposes*. 2005.

[86] J. Goldstein, D. Newbury, D. Joy, C. Lyman, P. Echlin, E. Lifshin, L. Sawyer, and J. Michael, *Scanning Electron Microscopy and X-ray Microanalysis*, vol. 1. 2003.

[87] T. Maitland and S. Sitzman, “EBSD Technique and Materials Characterization Examples,” in *Scanning Microscopy for Nanotechnology*, W. Zhou and Z. L. Wang, Eds. 2007, pp. 41–76.

[88] S. I. Wright, M. M. Nowell, and D. P. Field, “A Review of Strain Analysis Using Electron Backscatter Diffraction,” *Microsc. Microanal.*, vol. 17, pp. 316–329, 2011.

[89] A. Kelly, G. W. Groves, and P. Kidd, *Crystallography and Crystal Defects*, 2. Ed. New York: Wiley, 2000.

[90] D. Briggs and M. P. Seah, *Practical surface analysis. Vol. 1, Auger and X-ray photoelectron spectroscopy*, 2. ed. Frankfurt am Main: Wiley, 1990.

[91] K. H. Jack, “The Iron-Nitrogen System: the Preparation and the Crystal Structures of Nitrogen-austenite (γ) and Nitrogen-martensite (α’),” *Proc. R. Soc. A*, vol. 208, no. August, pp. 200–215, 1951.

[92] J. . Riviere, P. Meheust, J. . Villain, C. Templier, M. Cahoreau, G. Abrasonis, and L. Pranevicius, “High current density nitrogen implantation of an austenitic stainless steel,” *Surf. Coatings Technol.*, vol. 158–159, pp. 99–104, 2002.

[93] H. E. Du Plessis, “The crystal structures of the iron carbides,” University of the Free State (South Africa), 2006.

[94] H. Ferkel, M. Glatzer, Y. Estrin, and R. Z. Valiev, “RF plasma nitriding of a severely deformed high alloyed steel,” *Scr. Mater.*, vol. 46, no. 9, pp. 623–628, 2002.